공학박사 학위논문

Highly Stretchable & Transparent Supercapacitor based on Metal Nanowire Network Electrodes

금속 나노와이어 그물망 전극 기반의 고신축성 투명 슈퍼캐패시터 제작

2017년 8 월

서울대학교 대학원
기계항공공학부

이 하 범
(李 昰 範, Lee, Habeom)

Highly Stretchable & Transparent Supercapacitor based on Metal Nanowire Network Electrodes

지도교수 고 승 환

이 논문을 공학박사 학위논문으로 제출함
2017 년 8 월

서울대학교 대학원
기계항공공학부
이 하 범

이하범의 공학박사 학위논문을 인준함
2017년 6 월

위 원 장 : 최 만 수 (인)

부위원장 : 고 승 환 (인)

위 원 : 전 누 리 (인)

위 원 : 이 대 호 (인)

위 원 : 여 준 엽 (인)

Abstract

The upsurge in the use of portable electronics as well as diversification of consumer demands have been a strong driving force for development of innovative properties such as lightweight, flexibility and stretchability. In this regard, various energy storage or conversion devices on flexible substrate including batteries, solar-cells, fuel-cells and supercapacitors have been developed in order to maintain their performance under considerable physical disturbance such as bending, stretching and even twisting. Among those various energy storage devices, supercapacitor, owing to long cycle life with rapid charging and discharging capabilities at high power density, has become a most viable candidate to substitute conventional batteries. Actually, the researches related with the transparent, flexible and stretchable supercapacitors have been widely studied and focused in the carbon-based materials such as graphene and CNT. However, little research has been done on metal nanomaterials that are emerging as transparent, flexible, stretchable electrode materials.

In this proposal, we have studied the fabrication process of the next generation transparent, flexible and stretchable supercapacitor based on the metal nanomaterials. As a first step, we show that the efficiency of the flexible electrode manufacturing process can be increased by combining the roll-to-roll printing process and the laser sintering process. Furthermore, we develop a transparent and flexible electrode fabrication process using Ag nanowire network structure and establish a core shell nanowire synthesis process that can greatly improve electrochemical stability of the NW, confirming the possibilities of nanowire network-based electrode for the next-generation supercapacitor.

Keyword : Ag nanoparticle, Laser sintering process, Ag nanowire, Au-Ag core shell NW, Transparent and Stretchable electrode, Supercapacitor.
Student Number : 2014-30337

Table of Contents

List of figures

Chapter 1. Introduction

1.1. Background

In recent years, the demand for wearable electronic devices rapidly increased as consumers' demands have increased. Actually, the wearable electronic devices of the early type that do not require relatively structural changes such as wrist watches and glasses are already commercialized. However, it is expected that wearable electronic devices will ultimately be attached to the body and evolve in a form that maintains its original performance even when structural changes such as bending and stretching in accordance with human physical activity.[1-4]

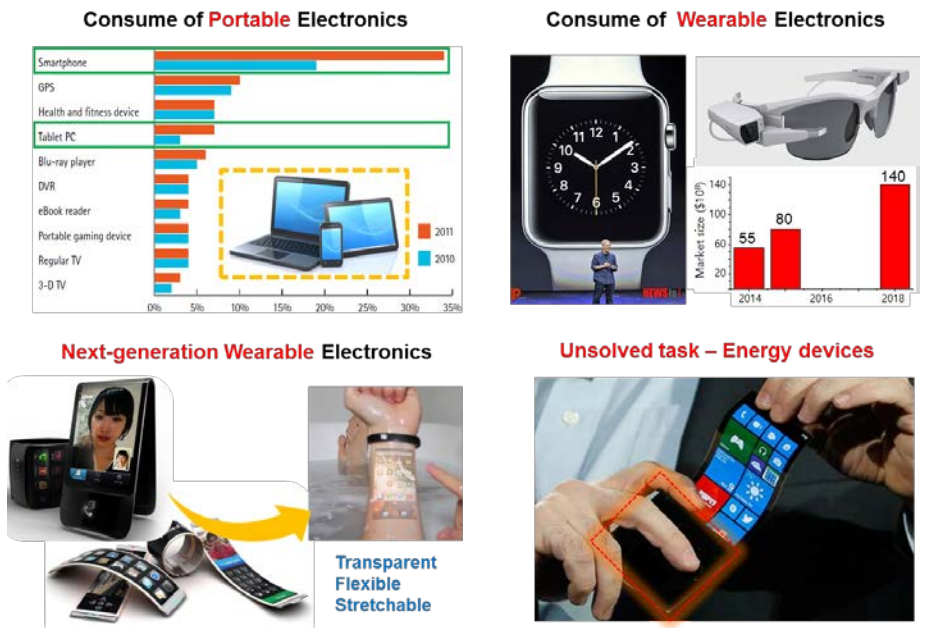

Figure 1. The motivation for evolution of energy devices of wearable electronics.

For all electronic devices, energy storage device that can supply operating energy is an essential element. Therefore, in order

to develop the ultimate next-generation wearable electronic device, it is necessary to develop an energy storage device capable of maintaining the performance even in structural deformation. Among various energy devices, supercapacitors (ultracapacitors, electrochemical supercapacitors) have received great attention in recent years due to their high-power density, long life cycle and high stability as candidate to substitute conventional batteries.[5-12] Supercapacitors are capacitors having a very large energy storage density compared to conventional capacitors, and could be largely divided into electrical double layer capacitors (EDLC) and pseudo capacitors.[13]

EDLCs store electrical energy through electrostatic charge accumulation and separation at the electrode and electrolyte interfaces. The net positive charges or negative charges are stored at electrode surface, at the same time, the same amount of opposite charges is accumulated near the electrode surface in the electrolyte. The aforementioned high-power density and fast charge / discharge characteristics arise from this energy storage mechanism. Also, the large energy storage density characteristics of the EDLCs result from the maximized surface area of the electrodes. A typical electrode material capable of providing huge surface area is a carbon-based porous material such as activated carbon, graphene and CNT. On the other hand, the pseudo capacitors store and supply electrical energy through faradic charge transfer through electrochemical redox reactions between electrodes and electrolytes. The pseudo capacitor has a much larger energy density than the EDLC because it also utilizes the charge accumulation through the redox reaction as well as the physical accumulation of the charge on the electrode surface.[14-16] As

the most common electrode material of the pseudo capacitor, metal oxide and a conductive polymer are used, and the materials store the electrical energy during the charging step, through a process of accumulating charges in a metal lattice and a polymer matrix, respectively.

Nowadays, without distinguishing the types of super capacitors, there have been active researches on fabrication of supercapacitors that are flexible, stretchable, and even transparent as interest and demand for wearable devices increase.[17-21] Most of these studies are based on carbon-based materials such as Graphene, CNT and carbon fiber. However, graphene or CNT requires a fairly high temperature and inert gas environment in their synthesis process, as well as post-treatment with toxic chemicals to ensure sufficient conductivity.[22, 23] Moreover, considering that metal nanoparticles and metal nanowires are very useful materials for fabricating flexible and stretchable transparent electrodes, it is unfortunate that these studies are biased toward carbon-based materials only. Of course, there are some limitations in the fabrication of supercapacitors using metal nanoparticles and metal nanowire based electrodes. In this study, we intend to establish transparent, flexible and stretchable electrode fabrication process using metal nanoparticles and metal nanowires, and further concentrate on fabricating transparent, flexible, and stretchable supercapacitors using the resultant electrodes.

1.2. Purpose of Research

In this study, we demonstrate Ag NP conductive film on a flexible PET substrate through R2R gravure offset method followed by fast selective laser sintering process without any conventional bulk heating post-process. The printed and laser annealed Ag NP electrode on a polymer substrate would be used for the current collector in a flexible all-solid-state supercapacitor. The electro chemical performance of the fabricated supercapacitor will be examined through various measurement methods. Moreover, the mechanical stability or the flexibility of the supercapacitor will be tested also, during long term repeated bending cycles to show that the laser sintering can successfully fulfill its annealing purpose to substitute the conventional slow thermal annealing process.

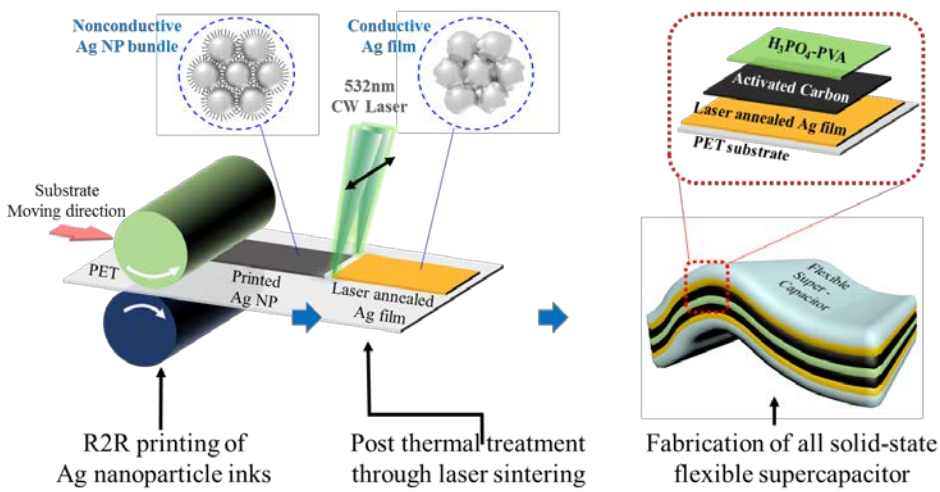

Figure 2. Schematic illustration of NP based flexible supercapacitor

Also later in this study, we will introduce a highly stretchable and transparent electrode intended for future wearable applications by constructing a partially embedded Ag NW percolative network on

an elastic substrate. Ag NW network, based on its superior electrical conductivity at high aspect ratios, has largely been studied as a stretchable or transparent conductor to date, but no attempts have been made toward a highly transparent and stretchable electrode for wearable electronics application. The Ag NW network electrode proposed in this study should exhibit not only superior optical transmittance and electrical conductivity comparable to ITO, but also outstanding electrical, mechanical and thermal stability withstanding 60 % strain which is the maximum strain value induced by the movement of the human body.

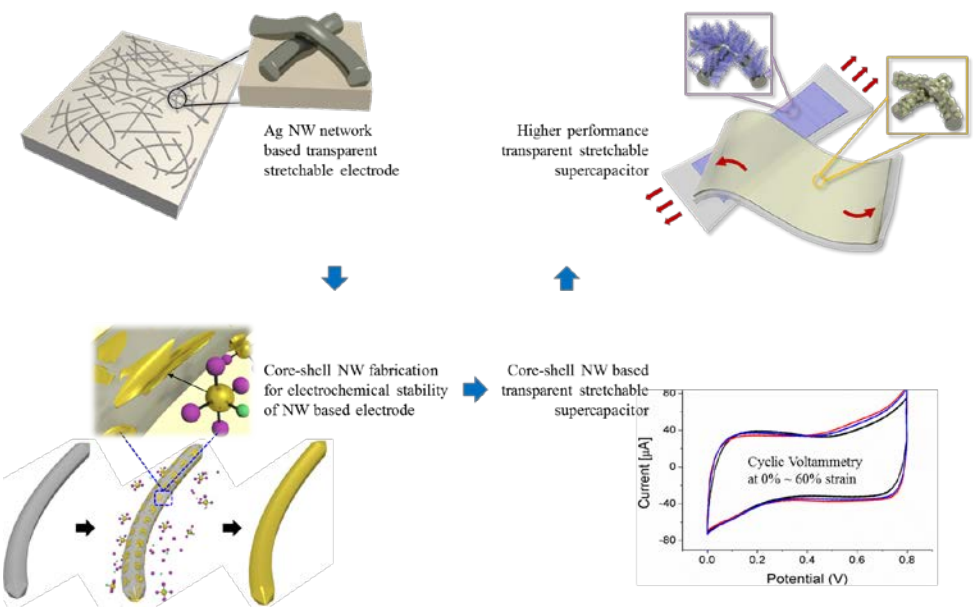

Figure 3. Schematic illustration of NW based transparent and stretchable supercapacitor

Although Ag NW is the one of the most promising candidate for transparent and stretchable electronics, its electrochemical instability has forbidden its application to the development of

electrochemical energy devices such as supercapacitors. We plan to develop a simple solution process to synthesize Ag-Au core shell nanowire can exhibit excellent electrical conductivity as well as greatly enhanced chemical and electrochemical stabilities compared to pristine Ag NW. The proposed core shell nanowire based supercapacitor have to processes fine optical transmittance and outstanding mechanical stability up to 60% strain. The Ag-Au core shell nanowire can be a strong candidate for future wearable electrochemical energy devices.

Chapter 2. Laser sintering of metal nanoparticles for fabrication of flexible supercapacitor

2.1. Combination of R2R printing with laser sintering process

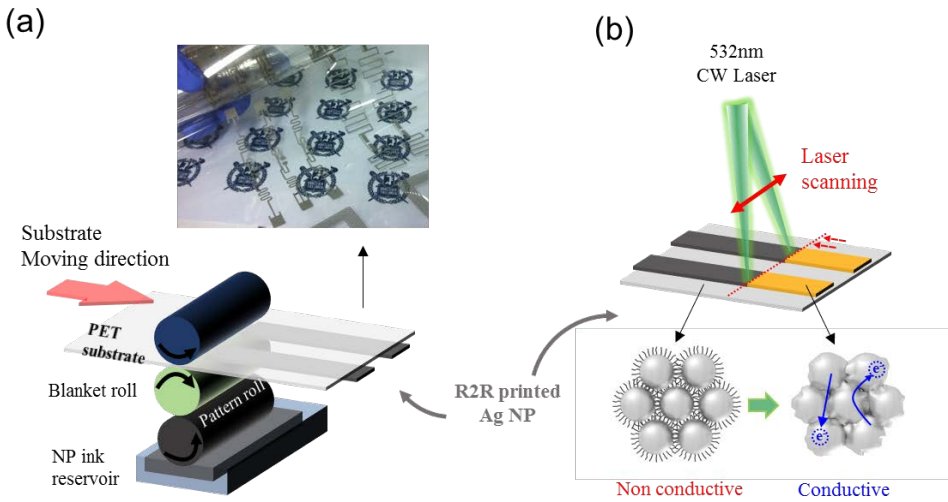

Figure 4. Schematic of combination of R2R printing and Laser sintering process

In this study, we propose a new heat treatment process that could replace the heat-wind drying process, which reduces the production rate and efficiency of the R2R printing process.[9, 24] The proposed new heat treatment process is the laser sintering process shown in Figure 4. Firstly, Ag NP ink (ANP, DGP-OS12000) is printed on a PET substrate by R2R gravure-offset printing process of three steps; Doctoring, Off and Set process. The speed of PET substrate passing through between blanket and impressing roll is fixed to 0.6 m/min and the printing force applied by the impressing roll is fixed to 15 kgf. After the printing process, the substrate is dried at 80 ℃ for few minutes to result in solvent free 400 nm thick Ag NP film. The photograph of the printed Ag NP

film is presented in Figure 4(a) as inset where Ag NPs are patterned in various shapes on the flexible PET substrate. The Ag NP film in this state is not electrically conductive, because the capping agent coated on the Ag NP surface blocks the contact between the Ag NPs and the movement path of electrons.

The transformation from distinct silver nanoparticle into continuous conductive film can be straightforwardly confirmed through the simple laser sintering process. The laser beam is selectively absorbed by the silver nanoparticles to generate optothermal heat, which removes the capping agent on the nanoparticle surface. This heat is low enough not to cause thermal damage to the PET substrate, because the part that absorbs the laser and generates heat is limited to the Ag NP layer. Actually, unlike the PET substrate, the silver nanoparticles melt by the heat, and the conductive continuous film is formed through the re-solidifying process.

2.2. Laser sintering of Ag NP film

For the laser annealing process, continuous-wave (CW) ND:YAG laser emitting 532 nm wavelength beam is applied, whereas the power is controlled by half-wave plate (HWP) and polarized beam splitter (PBS). The laser beam is expanded 5 times by beam expander (BE) and entered to the scanner (Scanlab, hurrySCAN II) consisting of a telecentric lens (f=100 mm) and two galvano mirrors which are driven by a computer software (SAMLight). The focused laser beam is scanned selectively at the square box area at 1,000 mm/s scanning speed with 200 mW power through the use of 2D galvano-mirror scanner. The change in

surface morphology of Ag NP layer immediately after the laser annealing procedure can be observed from the scanning electron microscope (SEM) analysis in Figure 5. It is apparent that the Ag NP layer which is underwent laser sintering is distinguishable from pristine Ag NP layer.

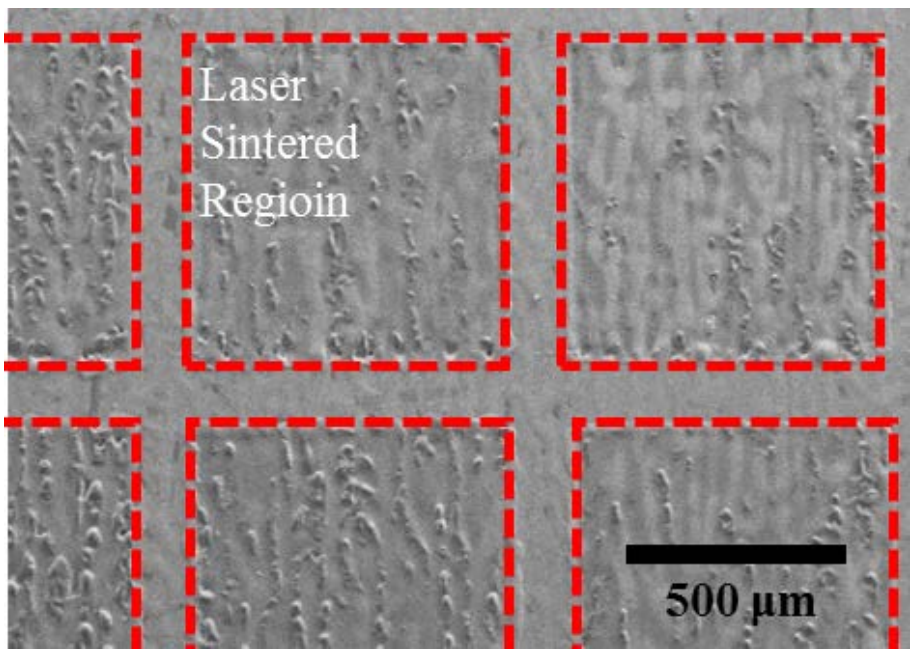

Figure 5. SEM image of laser sintered Ag NP film

Whereas the difference is more clearly noticeable from the high magnification images (Figure 6). The as-deposited Ag NP film is composed of Ag NP at diverse sizes up to ~100 nm, yet the resultant Ag NP layer after the laser annealing process shows more flattened surface with blurred boundaries, probably due to the complete melting and solidification of Ag NP through direct photo-thermal heating within the silver nanoparticle layer. The laser annealed silver nanoparticle layer not only exhibits excellent

electrical conductivity, but also superior adhesion to the underlying polymer substrate which is essential for the fabrication of stable energy devices.

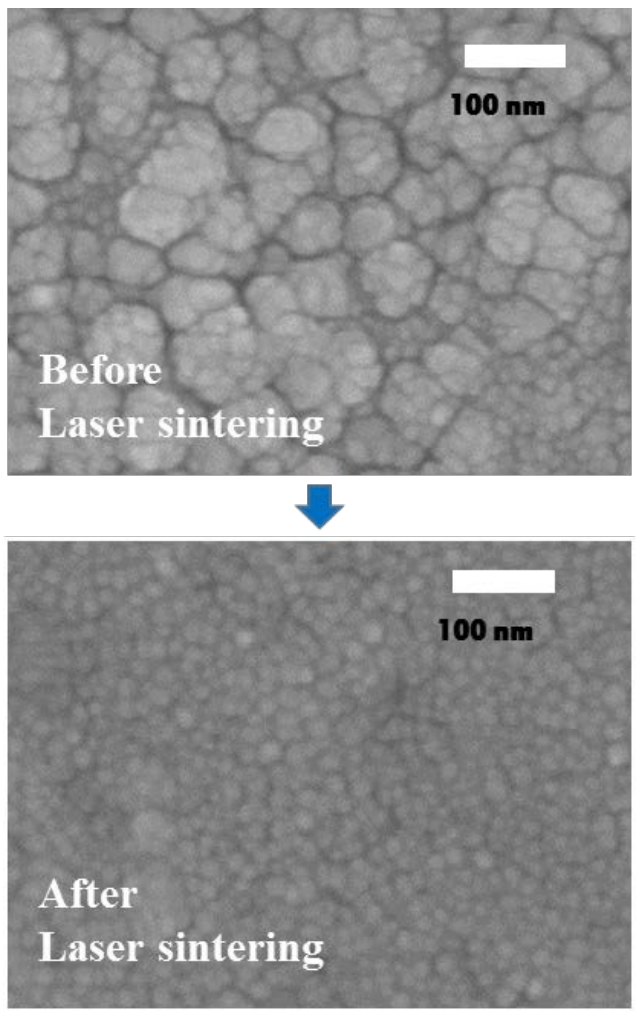

Figure 6. SEM images of Ag NP films before and after laser sintering process

2.3. Fabrication of flexible supercapacitor

In this study, flexible Ag NP based flexible electrodes which is prepared by R2R Gravure offset printing and subsequent laser annealing are used as a current collector for all solid-state flexible supercapacitor. The basic structure of a supercapacitor, which is similar to that of a battery, is shown in Figure 7.

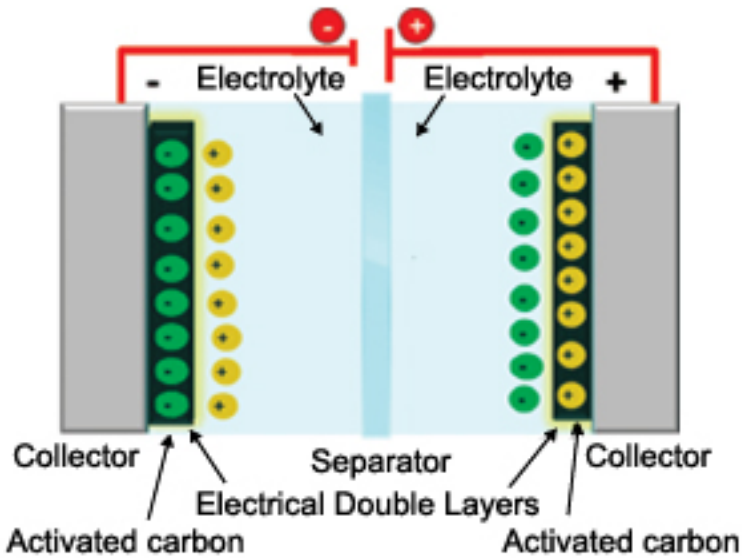

Figure 7. Basic structure of superpcapacitor

Two identical electrodes are combined with an electrolyte interposed there between and the electrode consists of a current collector and an active material. The electrode consists of a current collector and an active material. The current collector supplies electrons flowing from the outside to the active material layer, or vice versa. In this study, Ag NP electrodes serve as current collector, activated carbon is used as an active material and PVA-H_3PO_4 is used as an electrolyte. The detailed experimental process is as follows.

- **Preparation of activated carbon slurry**[9]: As a binder material, PVdF (Poly vinylidene fludride, Sigma Aldrich) is dissolved in NMP solution (1-Methyl-2-pyrrolidinone, Sigma Aldrich) under stirring at 60 ℃. After 3 hours, CEP21S (Power Carbon Technology) and Super-P (Timcal graphite & Carbon corp) are added to the solution and the whole mixture is stirred for another few hours. The mixing ratio of the three solutes is fixed to 1:8:1 in terms of weight, which is widely used in the previous studies. The total amount of the solutes in NMP solvent is 20 wt%.

- **Coating of activated carbon slurry on the Ag NP current collector**: The prepared activated carbon slurry is coated on the Ag NP coated PET film by doctor blading method and the coating amount is measured by an electronic scale after drying step. The amount of the active material is fixed to 1mg/cm^2 in every case.

- **Preparation of gel electrolyte**[25]: The polymer electrolyte is made by dissolving PVA (Mw 89,000~98,000, Sigma Aldrich) 6g and phosphoric acid (H3PO4, Sigma Aldrich) 6 g in 60 ml DI water with vigorous stirring at 85 ℃ for 3 hours.

- **Assemble of the supercapacitor**: A pair of carbon slurry coated Ag NP based electrodes are dipped into the gel electrolyte for 1minutes and the residual water is dried for 4 hours in the fume hood. At this time, as an external electrode, the one side of the electrode is connected to the copper tape with silver paste. After the drying process, the two electrodes are attached each other by being pressed. In this process, the dried gel electrolyte acts as not only adhesive but also as separator which prevent two electrodes connecting electrically.

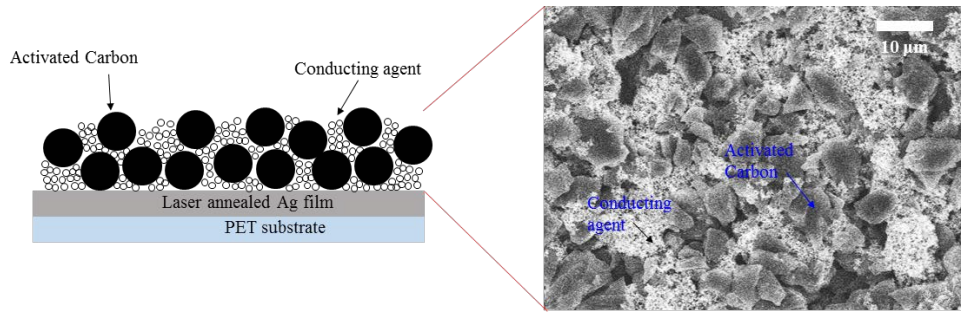

Figure 8. Structure of carbon slurry coated Ag NP film and its SEM image

Carbon slurry coated on the laser annealed Ag NP film contains both activated carbon as a working material and Super-p as a conducting agent to ensure sufficient electrical conductivity of the electrode as shown in Figure 8. The SEM image of the resultant electrode layer after complete drying procedure at 80 ℃ for 30 minutes, confirms that the activated carbon and the conducting agent are well deposited on the laser annealed Ag NP current collector.

2.4. Performance of the supercapacitor

In order to investigate the performance of the laser annealed conductive Ag film as a flexible electrode, we fabricated solid-state supercapacitor using the laser annealed Ag film, while another supercapacitor is assembled using conventional thermal annealed Ag film for comparison. For the thermal annealing process, the printed Ag NPs are kept for 2 hours at relatively low temperature condition (~100 ℃) to prevent any heat damage or thermal deformation of the underlying PET substrate. In the thermal annealing step, no apparent changes in morphology are observed at the Ag NP boundaries, unlike the laser annealed case. Figure 9

shows CV curves of the assembled supercapacitors based on the laser annealed and thermal annealed current collector, respectively, achieved at various voltage scan rates from 10 mV/s to 100 mV/s.

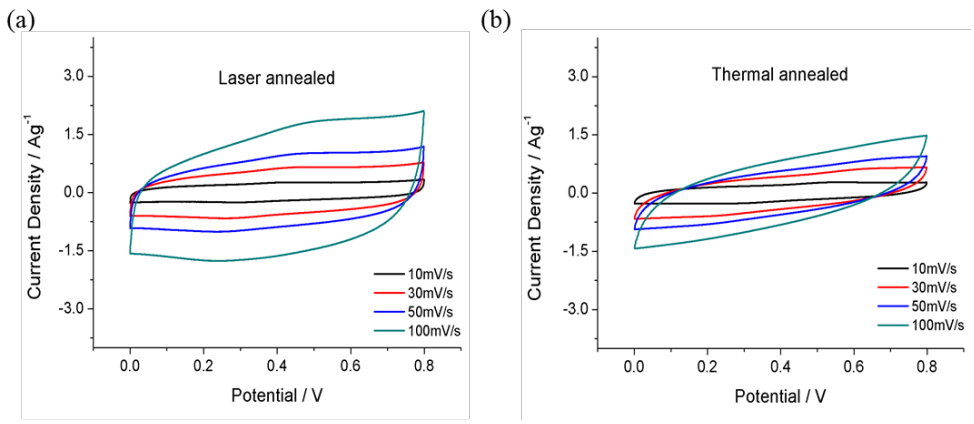

Figure 9. CV curves of the supercapacitors based on (a) the laser annealed and (b) thermal annealed current collector.

At lower voltage scan rate, both CV curves shows nearly rectangular shape indicating ideal capacitive behaviors.[26] However, as the voltage scan rate increases, the CV curves of two supercapacitors tend to be different. This phenomenon is more clearly shown in Figure 10, plotting both CV curves of each supercapacitor simultaneously. As it is apparent from the graph, the curve of the laser annealing case is more rectangular and the area enclosed by the curve is much larger than that of the thermal annealing case. This trend indicates that the supercapacitor using laser processed current collector has more ideal capacitive properties and bigger specific capacitance at equal conditions, since the electrical conductivity of the laser sintered Ag film is superior to that of the thermal sintered silver nanoparticle film. In addition, due to the blurred boundaries of Ag particles, we suppose that the

carbon slurry is more uniformly contacted with the Ag film current collector resulting in improved series resistance.

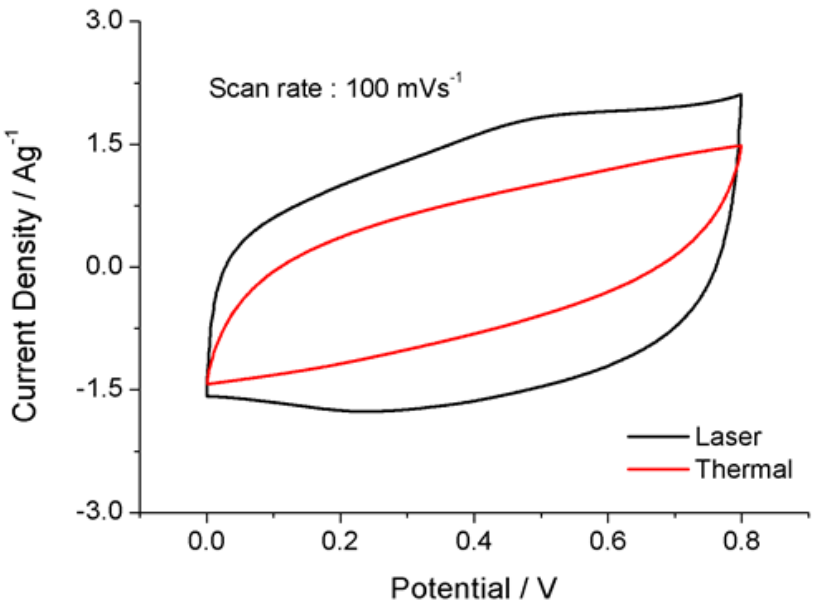

Figure 10. CV curves of each supercapacitor in 100mV/s scan rate

The specific capacitance at various scan rates are calculated through the following equation:[13]

$$C_{sp} = \frac{2}{m[V_2 - V_1]} \int_{t=0(V_1)}^{t(V_2)} i(v)dt$$

where, C_{sp}, v, i(v) and m are the specific capacitance, cell voltage, the current charging the cell at v and the weight of the active material, respectively. In our every experiment, the amount of the active material is fixed to 1mg/cm^2 and the integral term is calculated from the CV curve. Figure 11 indicates that the specific capacitance of the laser annealing case is larger than that of thermal

annealing case in every condition and also the decline of specific capacitance corresponding to the increase of scan rate is more suppressed.

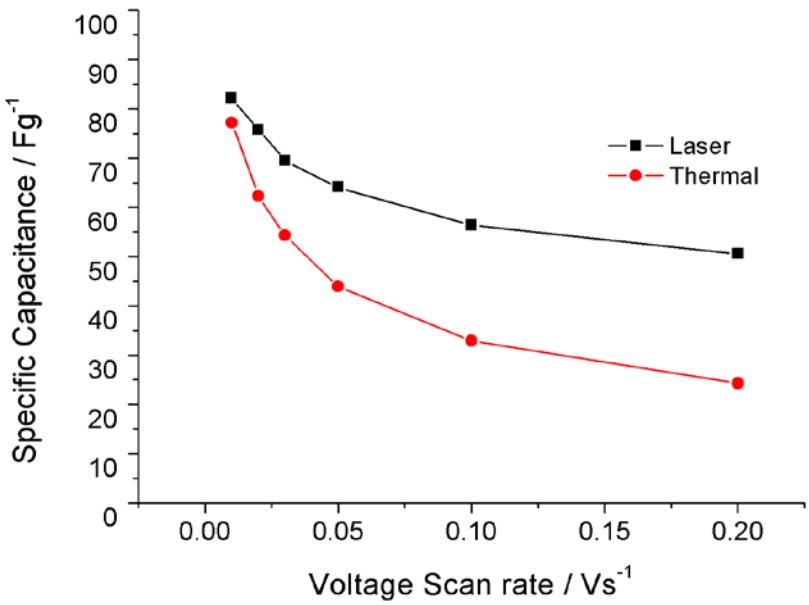

Figure 11. Specific capacitance at various scan rates gained from the CV curve

The energy and power density are most important parameters for evaluating a supercapacitor. Figure 12 shows the ragone plot related with energy and power density of assembled supercapacitor. Both of the energy and power density of our device are comparable to the latest reported high-performance solid-state flexible supercapacitor. In order to examine more detailed electrochemical properties of the supercapacitor based on laser sintered Ag NP film, the galvano static charge-discharge measurement is conducted at various current densities. The result presented in the inset of Figure 12 shows the typical triangular shapes at every current density condition. This result also confirms that the laser sintered R2R printed Ag film has outstanding electrical conductivity so that

the electrons move through the Ag film and to the active material easily.

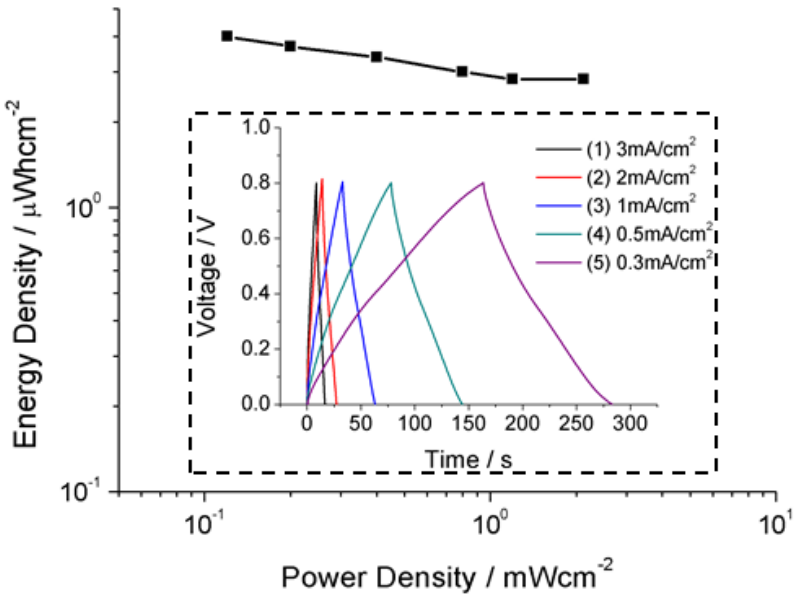

Figure 12. Ragone plot of the supercapacitor with charge-discharge curves at various current density as in inset.

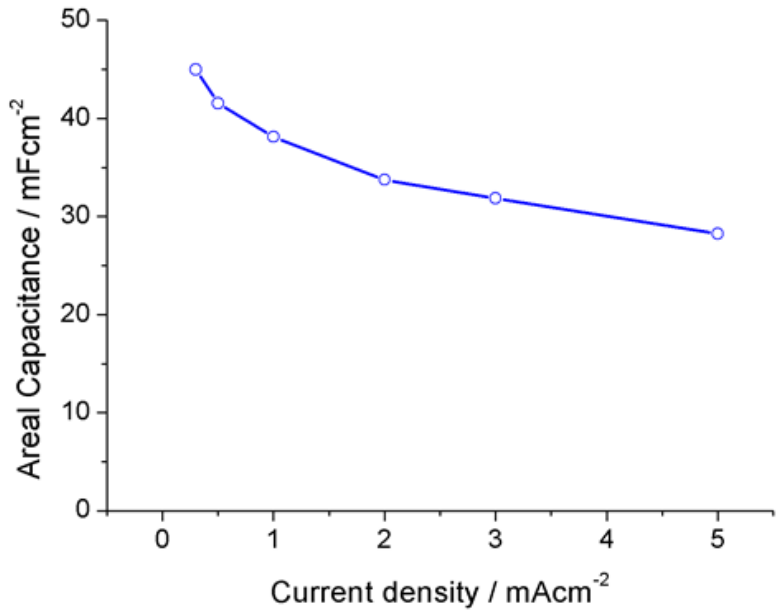

Figure 13. Areal capacitance at various current density

Also, the decrease of areal capacitance (calculated from charge-discharge curve) according to the increase of current density is found to be as small as the ones reported recently as it can be shown in Figure 13. The areal capacitance at 0.3 mA/cm^2 is 45 mF/cm^2 and slightly declined to 32 mF/cm^2 at 3 mA/cm^2.

We further probed the flexibility of the all-solid-state supercapacitor by drawing CV curves as the devices were bent to various bending angles at 0°-90°-135°-0°. Nearly rectangular CV curves in Figure 14 support that the supercapacitor can retain the ideal capacitive behavior even in the large bending condition.

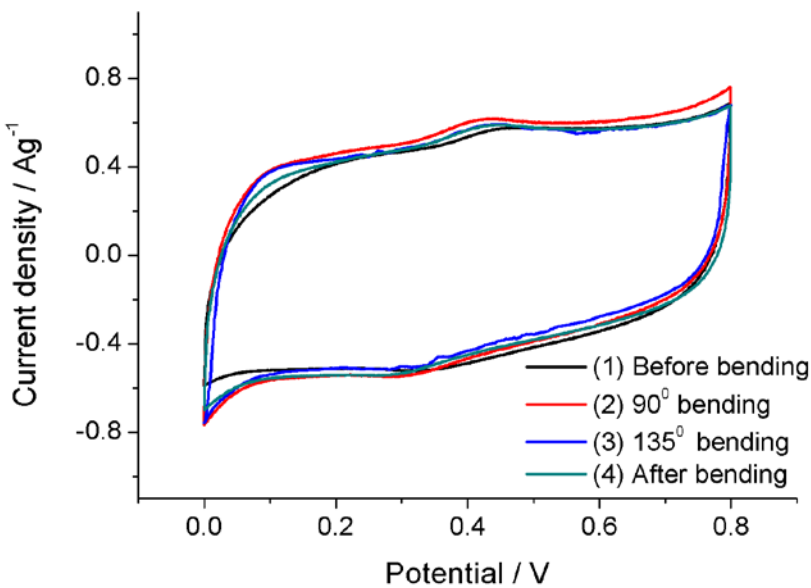

Figure 14. CV curves of the supercapacitor with different bending condition

In order to study the cyclic stability of the supercapacitor based on laser annealing, the assembled supercapacitor is examined by galvano static charge-discharge measurement at 5 mA/cm^2 for 1200 cycles under four different bending conditions. From the cyclic measurements, normalized capacitance is calculated as shown in Figure 15. Although the capacitance shows some fluctuation when the bending condition is changed, the solid-state supercapacitor retains 86 % of the initial capacitance after 1200

cycles even at various physical bending. The increase of the capacitance under the bending condition might be associated with the improved interfacial contact between Ag film current collector and activated carbon slurry,[27, 28] resulting in enhanced charge accumulation ability. The drop of areal capacitance in each bending step is presumed to be originated from the degradation of electrolyte and active material, resulted from the repetitive charge–discharge process that causes distortion of charge transport pathway.[29] The decrease in capacitance at 135° bending state is the largest, yet maintained 90 % of its initial capacitance which suggests that the laser annealed Ag film and its resultant supercapacitor exhibits fine flexibility and cyclic stability.

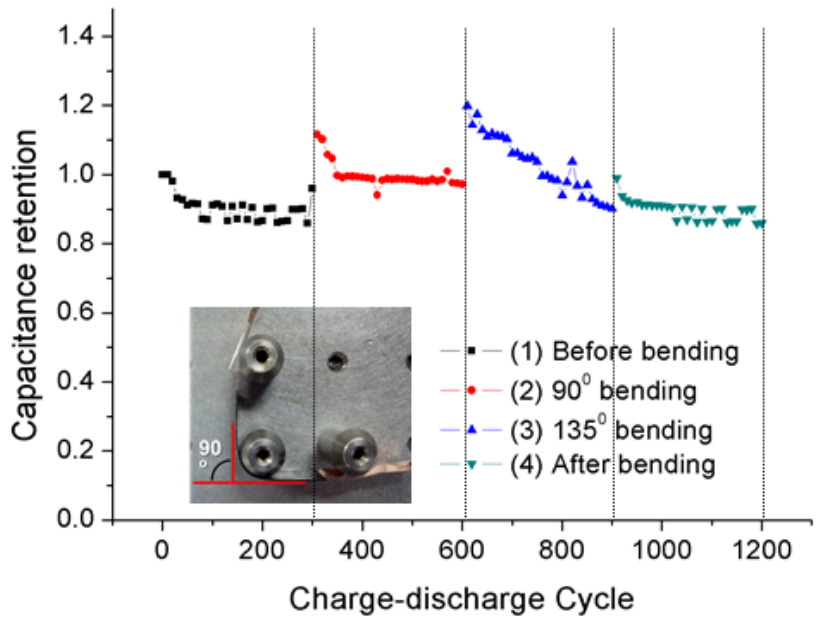

Figure 15. Normalized capacitance monitoring under repeated bending condition at various bending angle.

Finally, we connects three prepared supercapacitors in series to turn on a red light emitting diode (LED) so as to demonstrate the applicability of our supercapacitor as a power source of an actual device. After charging for 10 seconds at 2.4 V, the assembled supercapacitors could act as a power source of the LED as shown in Figure 5(a) over 30 seconds. Figure 5(b) and (c) show the CV curve measured at 100 mV/s voltage scan rate from 0 V to 2.4 V potential range and galvanostatic charge-discharge curve recorded at 1 mA/s charge current, which again show typical supercapacitor's behavior. These results clearly explain again that the laser annealed R2R printed Ag electrode could fuction as an excellent current collector for all-solid-state flexible supercapacitor.

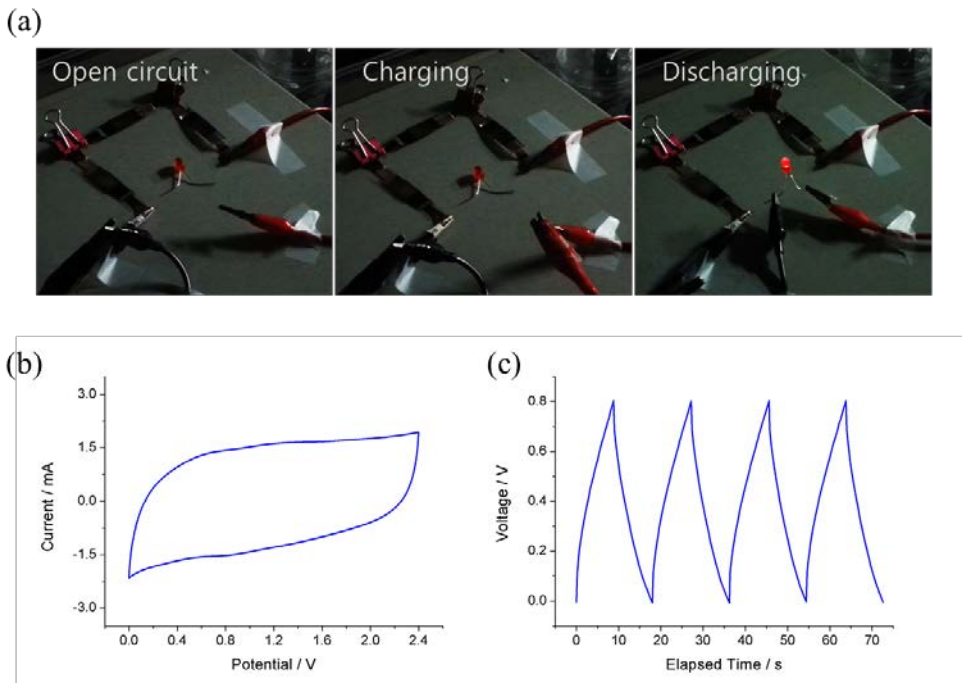

Figure 16. (a)Demonstration of a series-connected supercapacitors to power a red LED (b) CV curve and (c) charge-discharge curves of the series-connected supercapacitors.

As a result, we have successfully fabricated Ag NP conductive film on flexible PET substrate by R2R printing method followed by focused laser sintering post process. As Ag NPs are instantaneously melted and solidified by direct absorption of the scanned laser beam through low temperature photo-thermal process,[30-32] the resultant Ag NP film restores the bulk state electrical conductivity very rapidly without any thermal damage to the flexible substrate.[33] After coated with activated carbon slurry, the prepared flexible electrodes with Ag NP current collector and active material are sandwiched with a polymer medium layer (PVA-H_3PO_4) as both electrolyte and separator, to assemble flexible all solid-state supercapacitors that can operate even at bending state up to 135°. The supercapacitor shows ideal capacitive behaviors in various electrochemical study (Cyclic voltammetry and Charge-discharge test) and retains its performance even in 1000 times repeated bending without any severe decrease of capacity. It indicates that the laser annealing method could replace the conventional thermal method as an efficient post-processing for R2R printed metal NP electrode. So, by combining the proposed laser sintering method onto the existing R2R system, we expect that the productivity of flexible electronics could be improved to a great extent in terms of processing time and space.

Chapter 3. Ag nanowire network based transparent and stretchable electrode

3.1. Concept of Ag nanowire network electrode

Transparent conductor is an inevitable component for various optoelectronics such as solar-cell, electro chromic device, display, OLED and touch screen panel. A transparent electrode refers to an electrode that can transmit light, in particular a visible light region, in a direction perpendicular to a surface while allowing electricity to flow in parallel direction to the surface. The most typical transparent electrodes are ceramic based electrodes, which are made of thin film of conducting metal oxide materials such as ITO and FTO coated on transparent glass. In particular, as the ITO has a very high bandgap, it transmits most light in the visible light region and possesses sufficient charge transport material as an n-type semiconductor, thereby exhibiting excellent electrical conductivity as well. However, since the ITO reserves are limited, there is a limit to supply of materials and price competitiveness is low. Moreover, due to the nature of the ceramic material, it is fragile and not suitable as flexible electrode material.[34] In addition, the production of ITO electrodes has many room for improvement in terms of productivity because the conventional processes require high vacuum equipment such as physical vapor deposition, e-beam evaporation and sputter deposition or the harsh processing conditino.[35] Due to the above reasons, researches on transparent electrode materials for replacing ITO have been progressing actively.

These studies are largely divided into a study using a carbon-based material and a study using a metal material. In the case of a transparent electrode using a carbon-based material, it is manufactured by applying a very thin layer of graphene or CNT on a transparent substrate. However, in order to fabricate an electrode having sufficient electrical conductivity by utilizing graphene or CNT, a high vacuum, a high pressure, and a high cost process are required. Further, there is a problem that post-treatment, which use a highly toxic chemical, is required.

The transparent electrode based on a metal material is mainly formed by applying a metal grid having a fine line width on a transparent substrate. The metal has excellent electrical conductivity due to sufficient free electrons, but because it has the property to block the light including visible light, it is necessary to be a grid structure including voids to be a transparent conductor. There are various methods for fabricating a metal film patterned into a grid shape, such as imprinting, laser pattering, and vapor deposition using a mask. However, as these methods are accompanied by a waste of high priced noble metal such as silver, an alternative method is needed. In addition, the metal grid film fabricated with metal nanoparticle on the flexible substrate has limitation to be used for flexible electrodes. This is due to the fact that the metal grid could falls off the substrate in a repeated bending environment or cracks occur in the metal nanoparticle film. Actually, some research has been conducted on the fabrication of a strain sensor utilizing the fact that the electrical conductivity of the metal nanoparticle-based electrode changes abruptly according to the strain applied to the electrode.

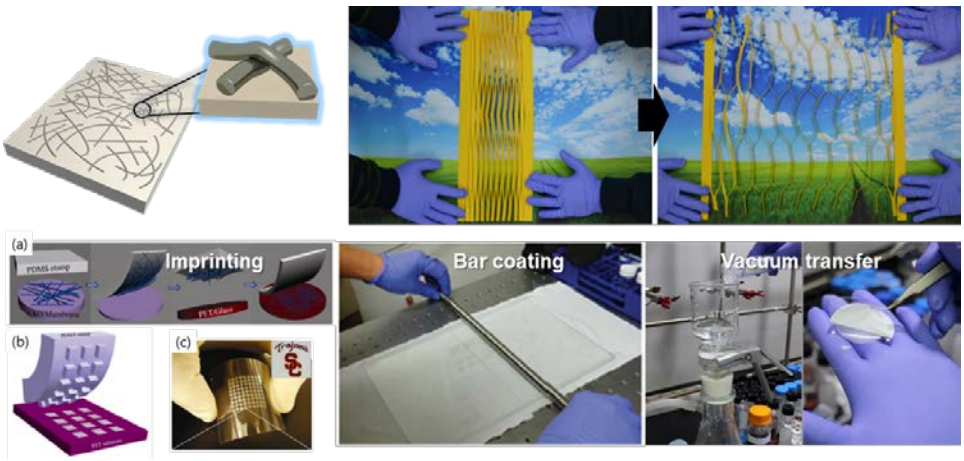

Figure 17. Concept and various fabrication methods of the Ag NW network structure.

Recently, metallic nanowire percolation network, using silver nanowire (Ag NW) especially, has been intensively studied and presented excellent results in terms of optical transmittance and electrical conductivity, even superior to ITO, as well as mechanical stability.[36-38] This is the result of combination of the excellent electrical properties of the Ag NW and the structural characteristics of the nanowire network. In recent years, due to the development of high aspect ratio Ag NW, which is over 100 micrometers in length, the performance of Ag NW based transparent and flexible electrodes has further enhanced. Nanowire network electrode manufacturing process includes vacuum transfer, spray coating, drop casting and Meyer rod coating. However, these processes require post treatment to restore conductivity after metal nanowire network structure formation, which reduces overall productivity and makes it impossible to produce electrodes on heat-sensitive substrates. As these problems, research on stretchable electrodes has not been actively conducted as compared with the study of flexible electrode fabrication because the stretchable substrates

such as PDMS and Eco-flex are much weaker to heat damage than the flexible substrate. That is, there is a need to study about new processes for fabricating transparent and even stretchable electrodes using Ag NW.

In this study, we propose a new method for fabricating transparent and stretchable electrode using Ag NW network structure. We also suggest a new concept of transparent and stretchable heater that can keep its performance at high strain condition to demonstrate the feasibility of Ag NW network based electrode for transparent and stretchable next-generation wearable device.

3.2. Fabrication of transparent and stretchable electrode

We newly establish and interpret the vacuum transfer method to fabricate the transparent and stretchable electrode. The solution filtration and transfer process, illustrated in Figure 18 has little waste of material and has the merit of adjusting of the transparency and electrical conductivity of the electrode very simply by controlling the concentration or amount of the nanowire solution used in the filtration process. The used Ag NW is prepared through the widely known polyol method, and its thickness and length are 100 nm and 100 μm, respectively. The prepared nanowires are dispersed in ethanol and used for the filtration and transfer process. The detailed procedure is as follows.

a) Nylon filter and PTFE filter are sequentially placed on the glass holder. Nylon filter acts as a buffer layer, and the size of the resultant Ag NW network is determined by the size of the holder.

b) Sufficient amount of ethanol is poured on the PTFE filter as a reservoir, followed by pouring the Ag NW solution, to ensure randomly distributed Ag NW network on the PTFE filter.

c) Target PDMS substrate is placed on top of PTFE filter for transfer of Ag NW network. The transfer can be either conducted in wet or dry condition. For wet transfer, PDMS is placed on the filter immediately after the complete filtration. On the other hand, for dry transfer, the filter is dried in room temperature for ~1 hour before the transfer. These two methods bring a substantial difference in the resultant microscopic feature. It will be treated later.

d) Detachment of the filter from the resultant Ag NW/PDMS composite, results the transparent and stretchable electrode.

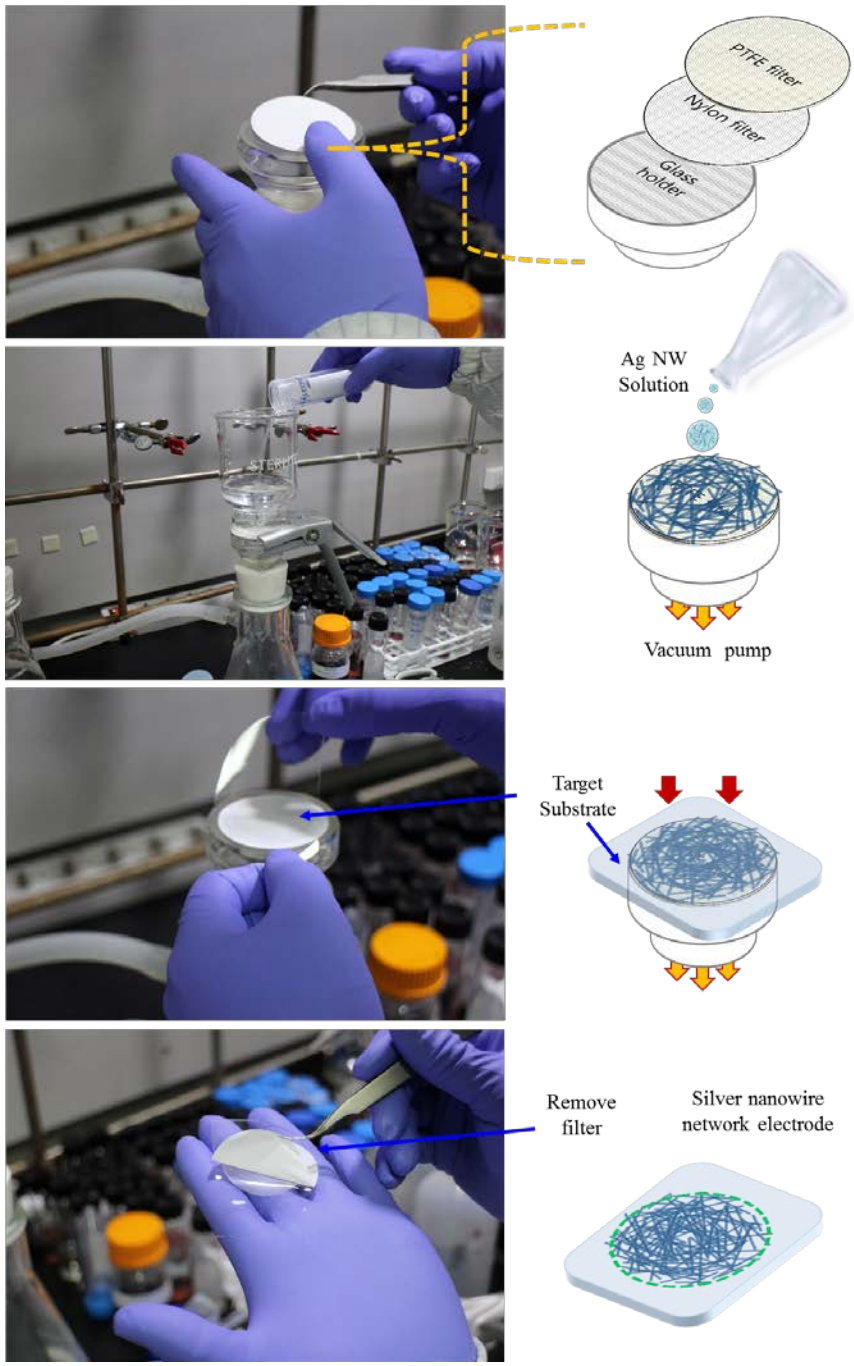

Figure 18. Illustration of vacuum filtration and transfer process

The Ag NW percolation network made by the suggested process exhibits excellent electrical conductivity without any post-treatment, which is considered to be the result of reduced contact resistance between the nanowires due to the pressure applied to the nanowire network during the transfer process. Considering that if the electrode is manufactured using the spray coating method or the drop casting method, some heat treatment processes for improving the contact resistance between nanowires evitable has to be required, it is shown that the suggested filtration and transfer method can largely simplify the nanowire network electrode fabrication process.

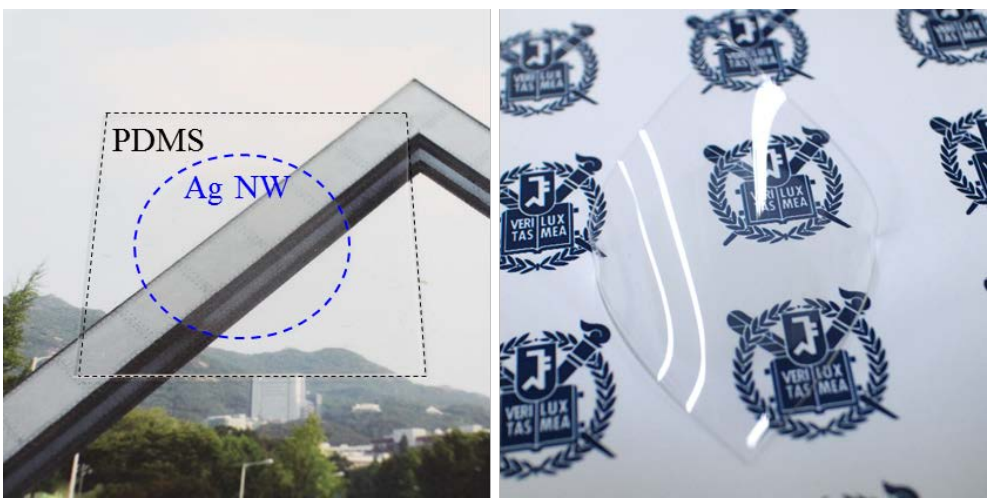

Figure 19. The transparent and flexible Ag NW percolation network / PDMS composite

Figure 19 is a actual images of the Ag NW / PDMS composite where the area subject to the Ag NW network transfer is denoted with blue dotted circle. It can be seen that the electrode is transparent enough for the background to be clearly seen through. Since the thickness of the Ag NW is around 100 nm, and much of

the total area of the electrode is not covered with the nanowires, the most of the optical transmittance of PDMS substrate are reflected to the electrode.

Besides, no apparent sign of degradation is found on either the PDMS film or the transferred Ag NW percolation network upon bending or twisting as shown in in the right photograph of the Figure 19. The robust mechanical stability of the electrode is believed to be due to the nature of the Ag NW network structure. In the SEM image, shown in Figure 20, we can observe the electrode structure composed with the Ag NWs, which has a very high aspect ratio.

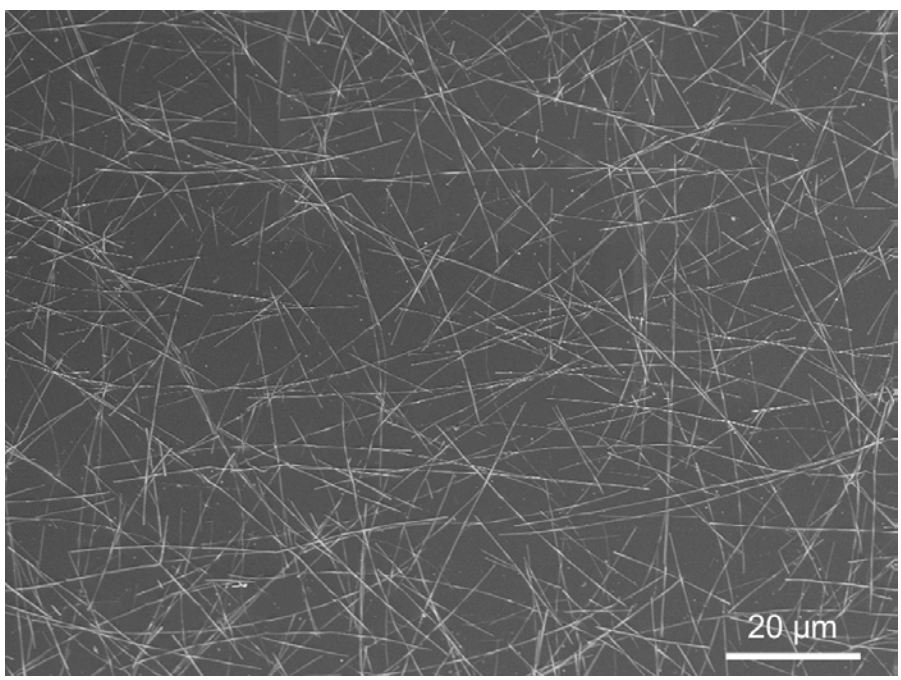

Figure 20. SEM image of Ag NW percolation network on the PDMS substrate.

As described above, the transparency and electrical conductivity of the electrode are determined by the concentration

or the amount of the Ag NW solution used in the filtration and transfer process. Figure 21 shows the electrical conductivity and transparency of the electrodes fabricated using several different amounts of Ag NW s. The used Ag NW which expressed in areal density are in the range of 132 mg/m2 to 528 mg/m2. It is confirmed that the total transmittance at 550 nm reaches 93 % for 132 mg/m2 when an empty PDMS at equivalent thickness is used as a reference, while the electrical resistance as well as the optical transmittance naturally decline as the density of Ag NW increases.

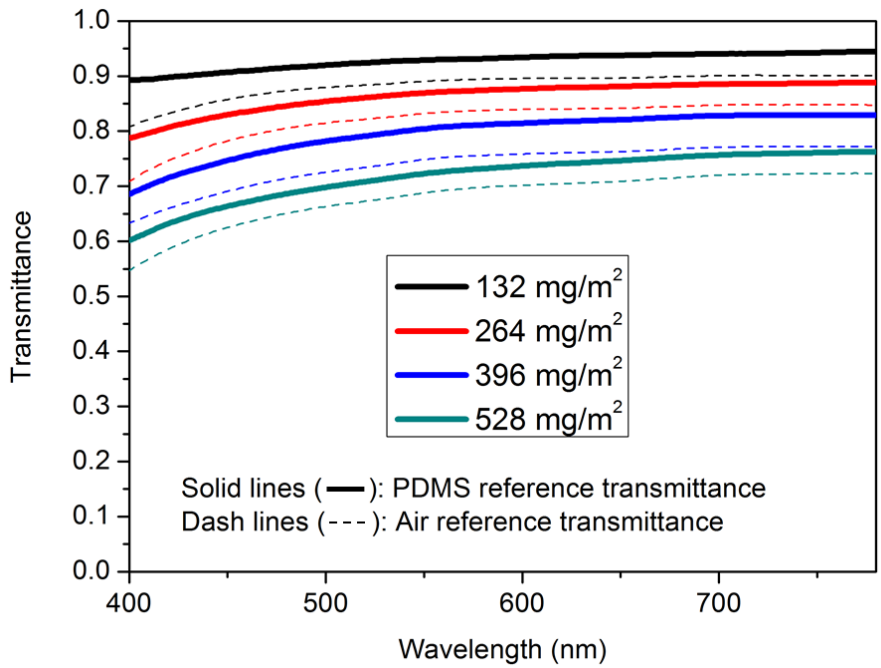

Figure 21. Transmittance of the Ag NW / PDMS composite electrode.

The strain-dependent electrical characteristics of Ag NW network electrodes are measured on a motorized stage at every 5 % strain for 5 cycles upon stretching and releasing. In every case, the resistance increases along with the applied strain, while the initial conductance is not fully recovered after a stretching/releasing

cycle as analogous to the electrodes with similar configurations. The strain dependent resistance stabilizes in a few stretching/releasing cycles, yet this aging process is much more rapidly completed for the electrode with higher Ag NW density. It is also notable that the increase in resistance compared to its initial resistance (R/R_0) is suppressed for the electrode with more Ag NWs as confirmed from the slope of the strain–resistance curve in Figure 22. Such small variation in the resistance at an applied strain, conceivably correlated to an increase in fused interconnections between Ag NWs is favorable for the realization of stretchable electronics with minimal change in performance. The Ag NW/PDMS electrode after the aging process still exhibits excellent optical transmittance and electrical conductivity (>85 % at 30 Ω/sq) which enable operation of a stretchable electronics at high optical transparency.

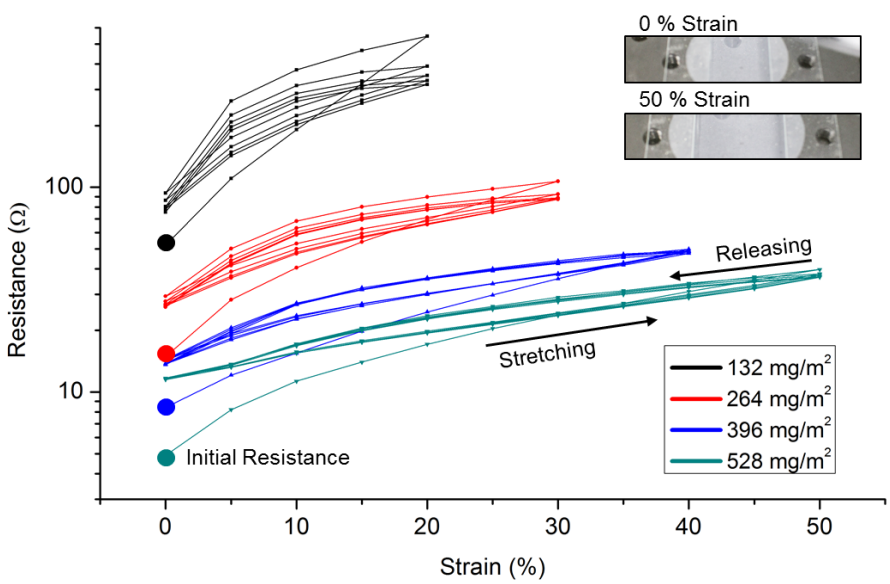

Figure 22. Strain–dependent electrical resistance of Ag NW percolation network eletrode under repeated stretching test.

One of the most important factors for manufacturing an electrode capable of stably maintaining electric conductivity even in such stretched state is the strong adhesion between the nanowires and the PDMS substrate. We have developed a very simple technique that can greatly improve the adhesion between nanowires and PDMS substrates. In the Figure 22 showing the enlarged SEM image of the Ag NW on the PDMS substrate, it can be seen that the nanowires are partially buried in the PDMS substrate, and this phenomenon occurs mainly in the overlapping part of two or more nanowires.

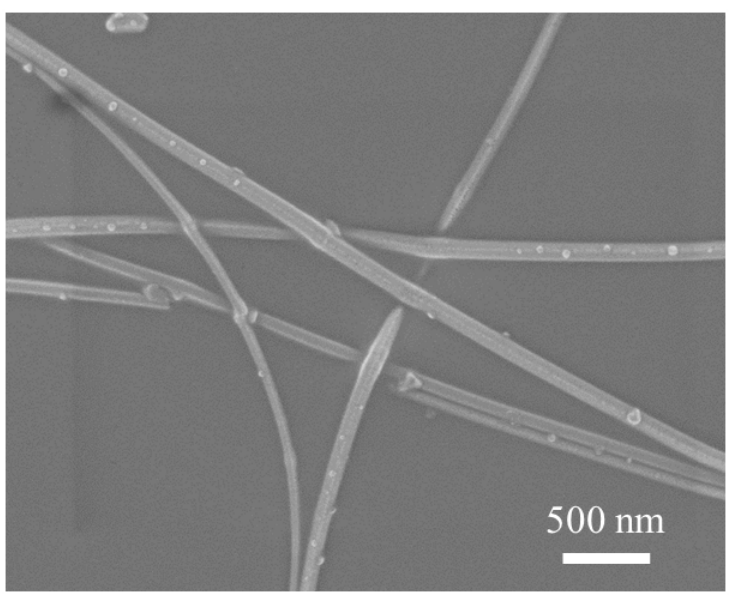

Figure 23. SEM image of Ag NWs on the PDMS substrate.

The structure in which the nanowires are partly buried in the substrate can greatly improve the adhesion of the nanowire network electrode onto the PDMS substrate, and thus, even if the electrode is subjected to mechanical deformation such as bending or stretching, thereby it is capable of maintaining the overall structure stably.

This unique morphology is most likely originated from the combined effect of vacuum pressure and solvent evaporation during the transfer process (see the Figure 19). The swelling of ethanol to pristine PDMS is known to be almost negligible, yet the absorption of ethanol vapor at the oxidized PDMS surface causes a noticeable compressive stress at the interface. Since the pressure is constantly applied between Ag NW and the PDMS layer during the transfer process, the compressive stress at the PDMS surface, stemming from the solvent evaporation, is likely to be concentrated and relaxed by wrapping the Ag NWs.[39] This partial embedding of nanowires cannot be observed on a rigid substrate such as glass, and the Atomic force microscopic (AFM) observations of Ag NW networks formed on glass and PDMS are shown in Figure 24.

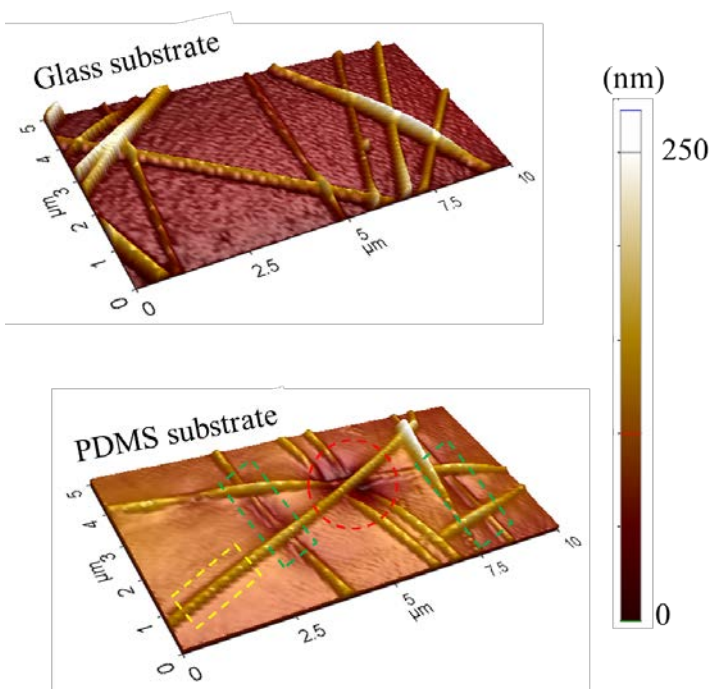

Figure 24. AFM profile of Ag NWs transferred on glass substrate (G) and PDMS (P).

To support the idea for generation of partially embedded

nanowire structure, one more AFM measurement is conducted about the Ag NWs transferred to PDMS layer at completely dry condition and the results are included in Figure 25.

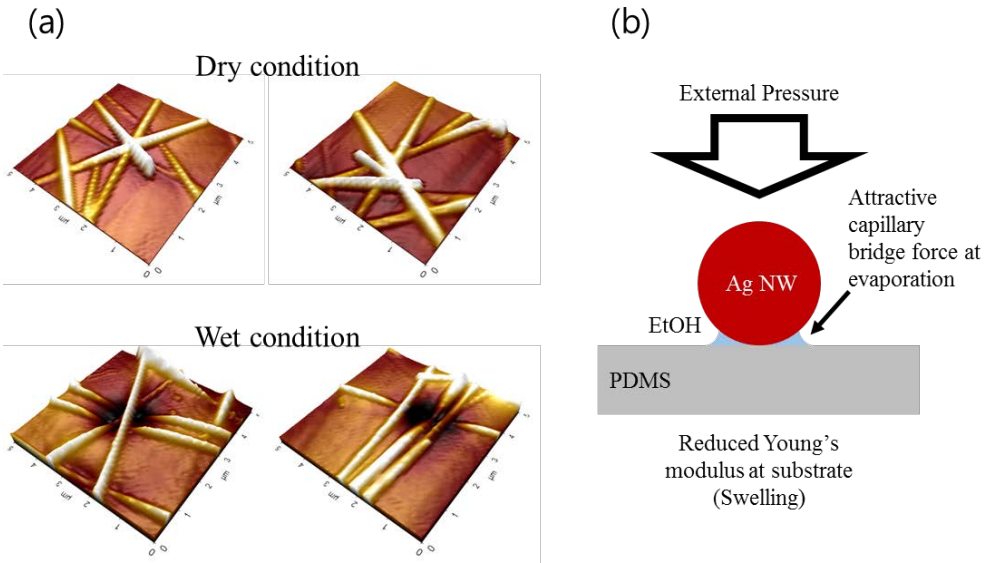

Figure 25. (a) AFM profiles of Ag NWs transferred on PDMS substrate at wet and dry condition, (b) The forces inducing the Ag NW embedding into the PDMS substrates.

It shows insignificant embedment of Ag NWs into the PDMS layer even at the nanowire junction when the ethanol is completely dried. The difference in the amount of embedment can also be explained with the same argument. Assuming that the initial vacuum pressure is spatially uniform throughout the PDMS layer, the larger surface roughness at the regions with higher Ag NW density or nanowire junction creates greater local pressure to cause strengthened embedment at the corresponding spot. Also, the sessile solvent at the nanowire junction might lend additional support to the attractive force between Ag NWs and PDMS layer at evaporation[40] to induce more definite features. Remarkably, this

phenomenon very much resembles the plasmonic welding process[41, 42] whose photo-thermal effect is very much enhanced only at the NW junction. The embedment of Ag NWs into the PDMS layer is supposed to provide higher mechanical stability as the surrounding elastomer with compressive stress grasps the adjacent Ag NW to yield better adhesion between the two structures. The figure 24 confirms the adhesion enhancement of the Ag NW network electrode to the PDMS substrate.

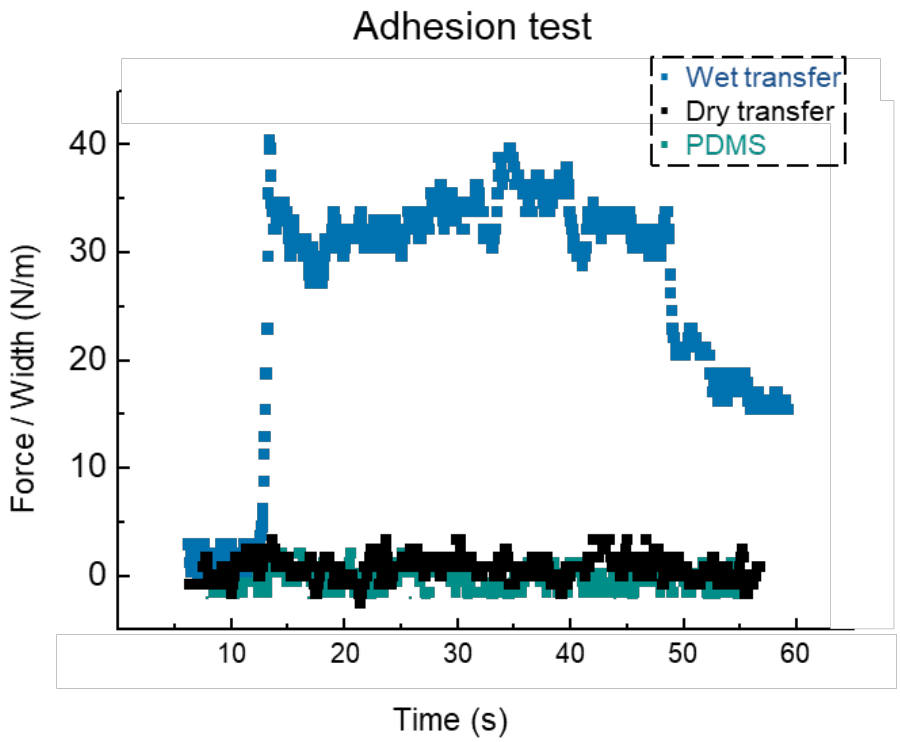

Figure 26. Comparison of the adhesion force of Ag NW network with PDMS substrate between wet and dry transfer.

3.3. Fabrication of transparent and stretchable heater

Here, we demonstrate a highly Stretchable and Transparent Ag NW (STAN) heater for wearable electronics applications for the first time based on partially embedded Ag NW percolation network on PDMS substrate that operates under strain over 60 % and other real-time deformations commonly associated with human motion such as bending and twisting.

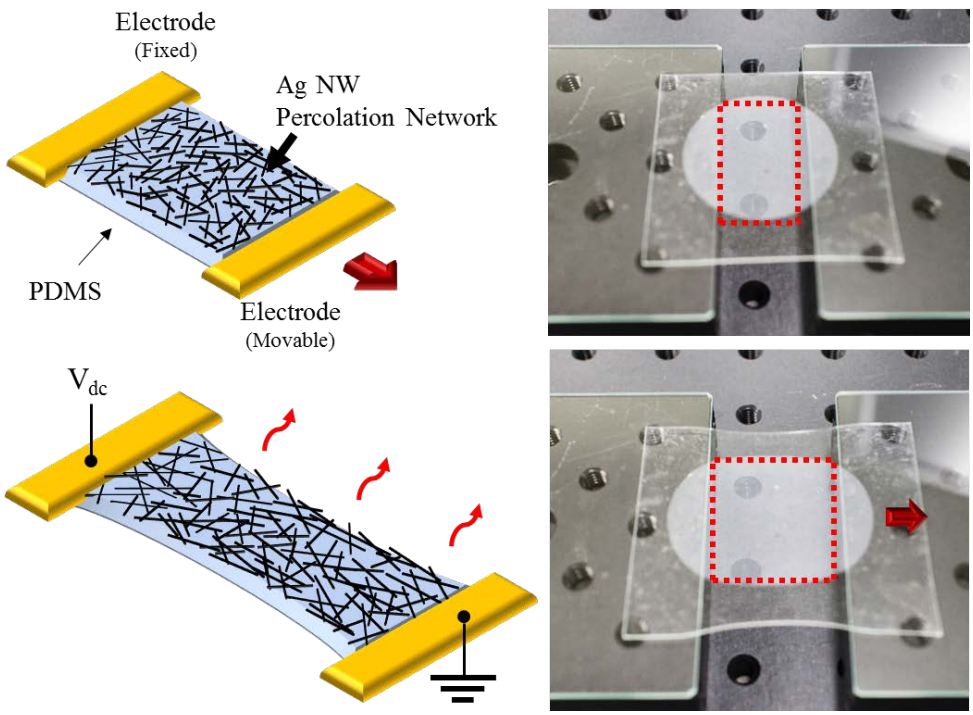

Figure 27. Schematic illustration of STSN heater and the photographs of Ag NW network electrodes of which ends are attached on the glass connected to the moving stage.

The schematic illustration of STAN heater and the photographs of Ag NW network electrodes of which ends are attached on the glass connected to the moving stage is suggested in the Figure 27.

Using the property of PDMS firmly attached to the glass, both

ends of the Ag NW electrodes are fixed to the respective glass substrates. And the one of two-glass substrate is attached to the fixed stage and the other is attached to the movable stage. And the external circuit are connected to the electrode by copper tape with silver paste, in this process the copper tapes are attached on the region of PDMS placed on the glass to prevent exposure to strain.

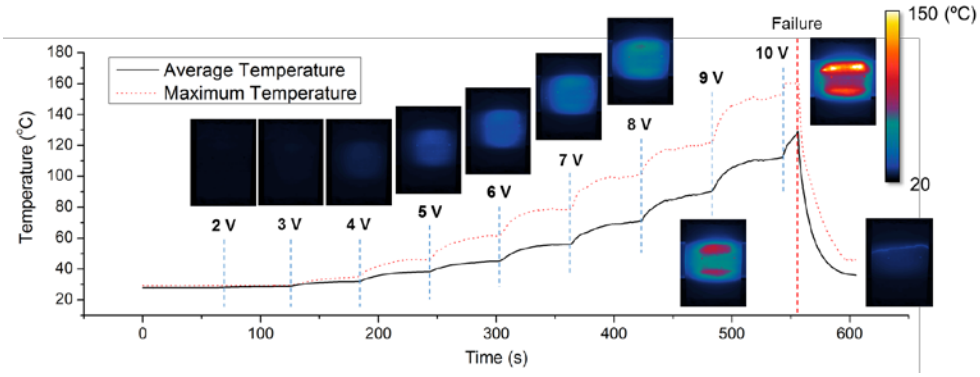

Figure 28. Transient temperature evolution of STSN heater under zero strain at stepwise voltage rise from 2 V to 10 V.

As a constant DC voltage Vdc is applied at the Ag NW network electrode, electrical current flows through the Ag NW to induce resistive Joule heating that raises the temperature nearby. Since the joule heating characteristics are determined by the amount of current flowing through the electrodes, the area density of the Ag NWs is fixed to a value in following experiment. As shown in Figure 26, the Joule heating characteristics of the STSN heater are examined for 132 mg/m2 Ag NW density. Constant DC bias voltage is applied between two side ends of the target electrode, while the voltage is increased by 1 V every 1 min until the heater fails. Time dependent temperatures at various applied voltage are presented in

Figure 28 together with the corresponding temperature distribution captured by IR camera as insets. The average temperature at the heating region is always lower than the maximum temperature with a smoother curve, and the increase in temperature is roughly proportional to the square of applied voltage as predicted. At 10 V bias voltage, we conjecture that the local temperature exceeds 200 °C at the moment of failure according to extrapolation from preceding data. The lower and upper operating temperature limits for PDMS are not well defined, but it is widely accepted that PDMS can withstand temperatures above 200 °C due to high thermal stability resulting from the strong siloxane bond. Since the temperature range required in general wearable applications is much lower, the thermal stability of the STAN heater is estimated to be appropriate for our purpose. Besides, the distorted temperature profiles at the high voltages in Figure 28 insets are not from substrate damage, but due to the highly non-uniform surface from sagging of the underlying PDMS layer as it expands at high temperatures and deviates from the focal plane of the IR camera.

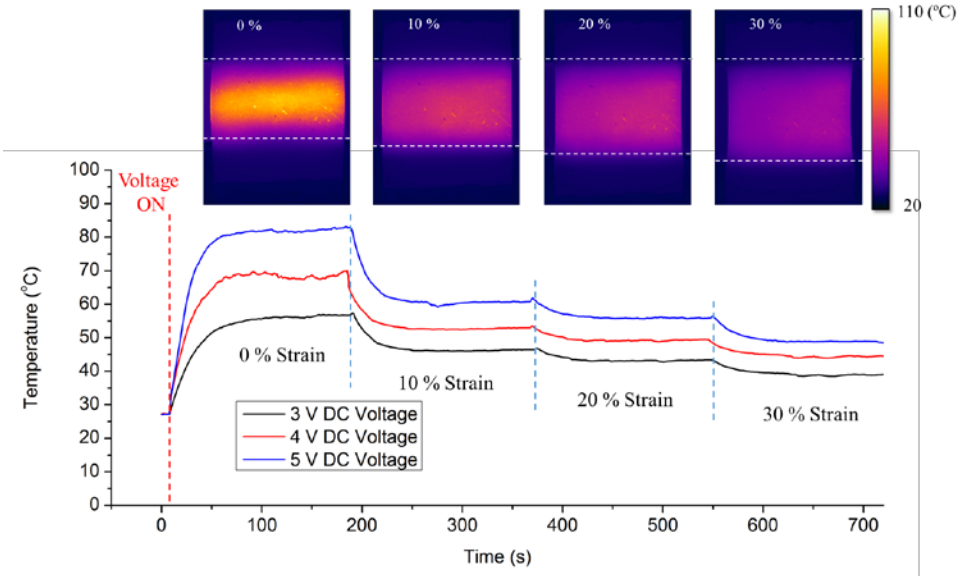

Figure 29. Transient temperature evolution of STSN heater under stepwise application of 0 to 30 % strain at various constant voltage.

The performance of the STSN heater is confirmed by applying step-wise tensile strain to the heater in real-time under a constant bias voltage. For the stretchable heater test, the Ag NW network electrode with higher areal density of Ag NW at 396 mg/m^2 has been employed to enable efficient heating at low voltage. The temperature changes according to the applied strain at 3, 4 and 5 V DC bias voltage are recorded in Figure 29 while the strain is increased up to 30 % with 10 % increments every 3 minutes. The STSN heaters exhibit rapid response in temperature upon the application of voltage and converge to a plateau in relation to the applied voltage. When a tensile strain is applied, the STSN heater works stably at a reduced temperature because heat generated by Joule heating at a fixed bias voltage is inversely proportional to the resistance of the target electrode and strained Ag NW network increase resistance.

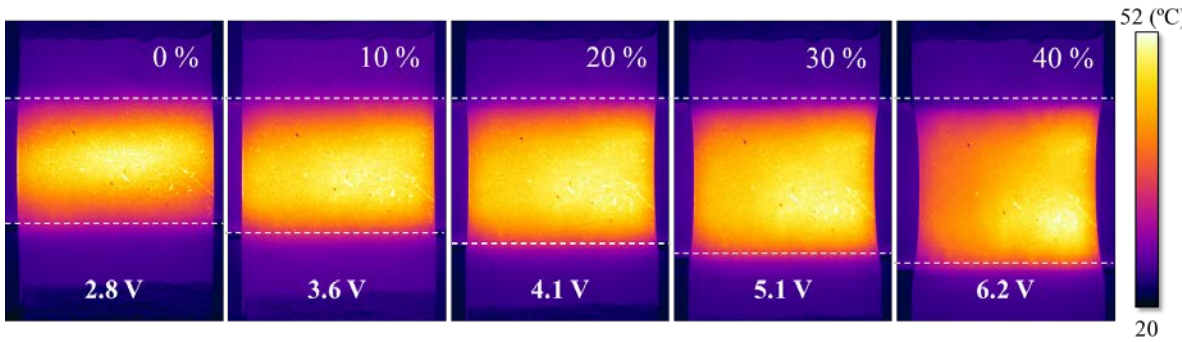

Figure 30. Temperature distribution of STAN heater under various strain with adjusted voltage to maintain constant temperature 50 °C.

The change in temperature, along with the strain, is unavoidable even at constant resistance as the increase in the surface area also affects the maximum temperature of the heater. As a result, the temperature can be held constant at an arbitrary strain only by adjusting the applied voltage through a feedback module. In Figure 30, the temperature of STAN heater is maintained constant at 50 °C while stretching by applying a different voltage at each strain.

Uniform heating has been regarded one of the most important criteria in electrical heaters, but only little attention has been paid to the selected area local temperature distribution control although it is common and more severe in large strain conditions (See figure 30) and even very important for some specific wearable applications.

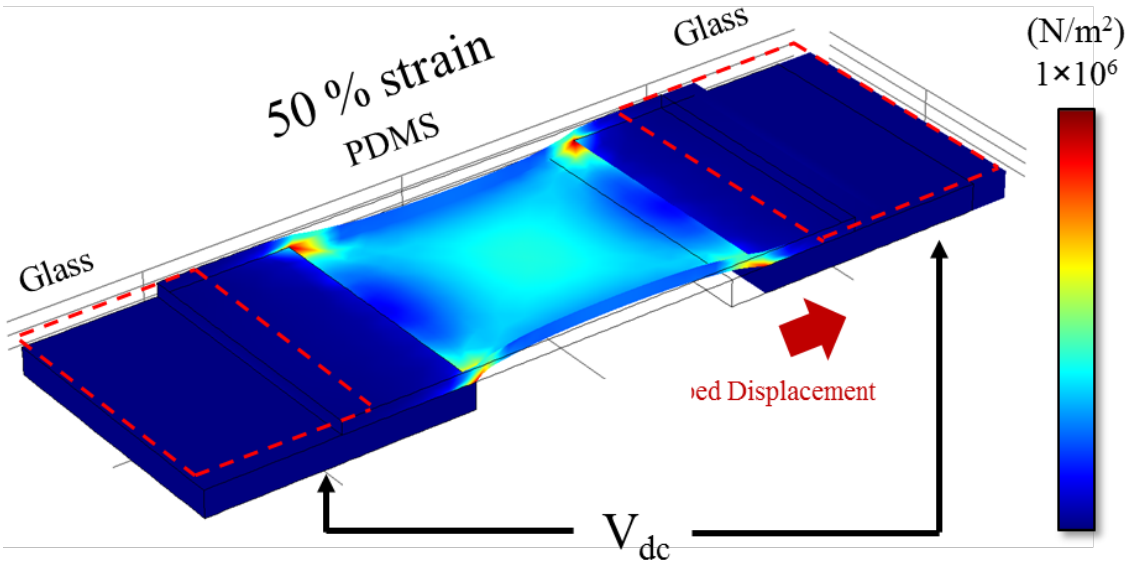

Figure 31. Stress simulation on PDMS layer at a large strain condition.

COMSOL simulation is conducted on von Mises stress at the surface of PDMS layer when an engineering tensile strain at 50 % is applied by widening the gap between two supporting glass substrates. As the effective stress is highly concentrated at the corners, the current primarily flows through the midway and the subsequent voltage drop as well as the resistive heating mostly happens at the center of the PDMS layer.

Likewise, manipulation of current density is often necessary for some specific wearable applications since temperature profile can be distorted under an arbitrary strain or mechanical deformation. As Ag NW is partially exposed to air in the Ag NW network / PDMS electrode, its spatial current density, and hence the resultant temperature profile, can be easily manipulated in STSN heater through selective laser ablation patterning of Ag NW network. Laser ablation is directly applicable to Ag NW network electrodes at ambient conditions without damaging the underlying PDMS layer due to high spectral transmittance of PDMS[43] and low laser ablation fluency threshold of Ag NW.[44]

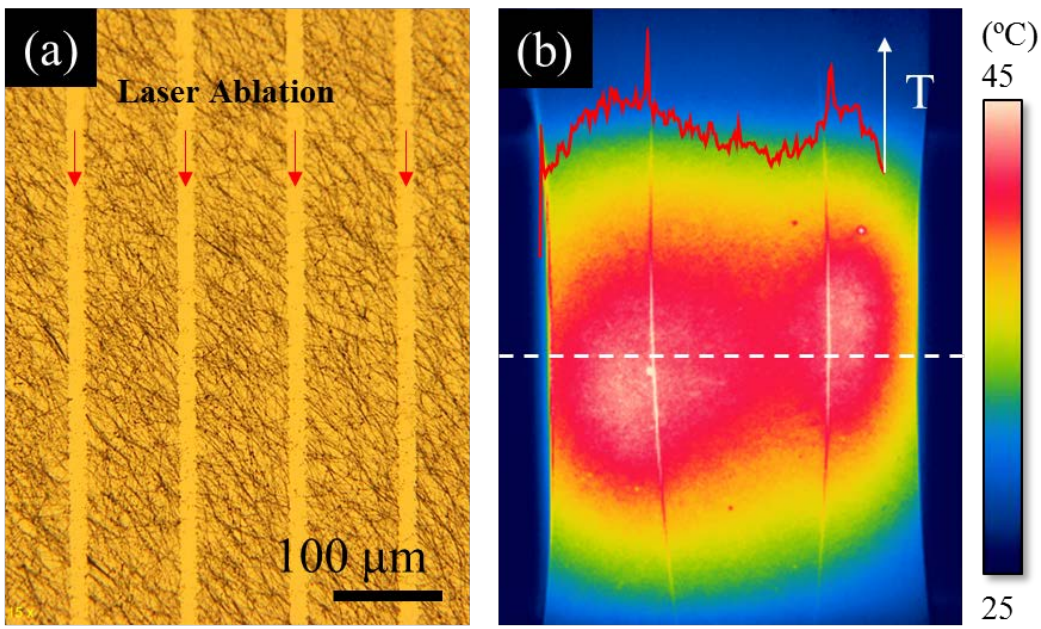

Figure 32. Optical image of patterned Ag NW on PDMS by selective laser ablation and temperature distribution image of the STSN heater.

Without using any conventional photolithography step, Ag NW can be selectively and completely removed at micro-scale along the desired path without any observable damage as shown in Figure 32 (a). And as an example of temperature profile modulation, two ablation lines are created on the Ag NW network electrode to define a concave electrical path in the interior, so that the current density shrinks at the center of the target electrode. As a result, at the 50% strain condition the maximum temperature of the STSN heater is no longer at the midpoint, whereas the cross-sectional temperature profile at the bisecting line shows two maxima as shown in Figure 32(b) along the white dotted line.

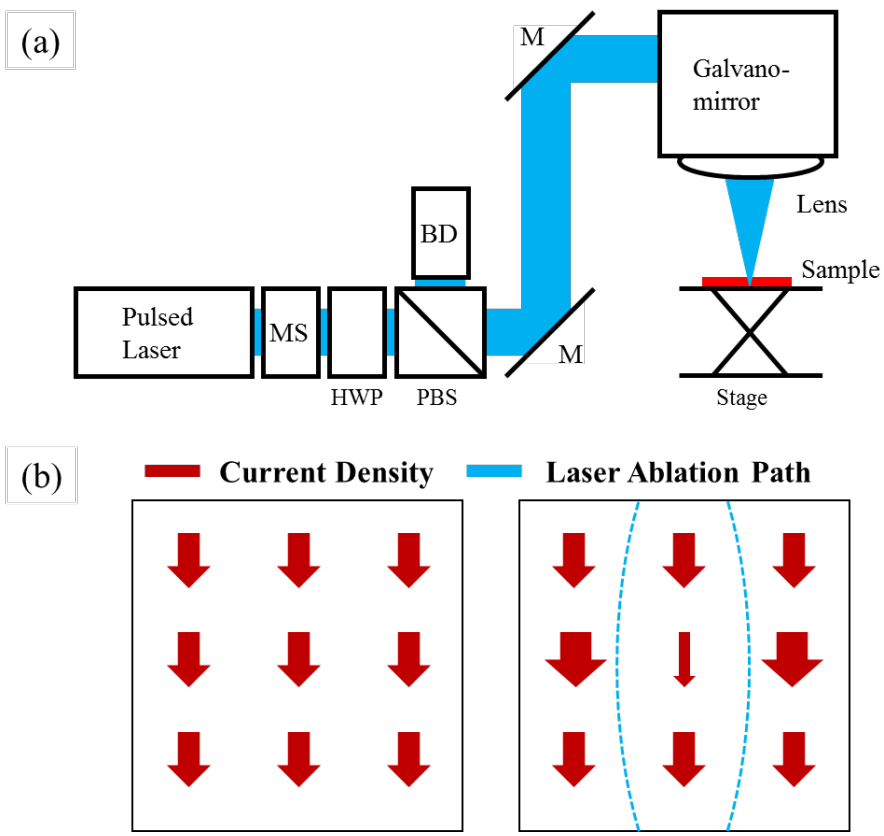

Figure 33. Experimental setups for laser ablation and electrode designs for temperature manipulation.

The experimental setup for laser ablation is included in the Figure 33 (a) (MS: Mechanical shutter, HWP: Half-wave plate, PBS: Polarized beam splitter, BD: Beam dump, M: Mirror). The presumed current density of Ag NW / PDMS electrode before and after the laser ablation patterning are shown in Figure 33 (b).

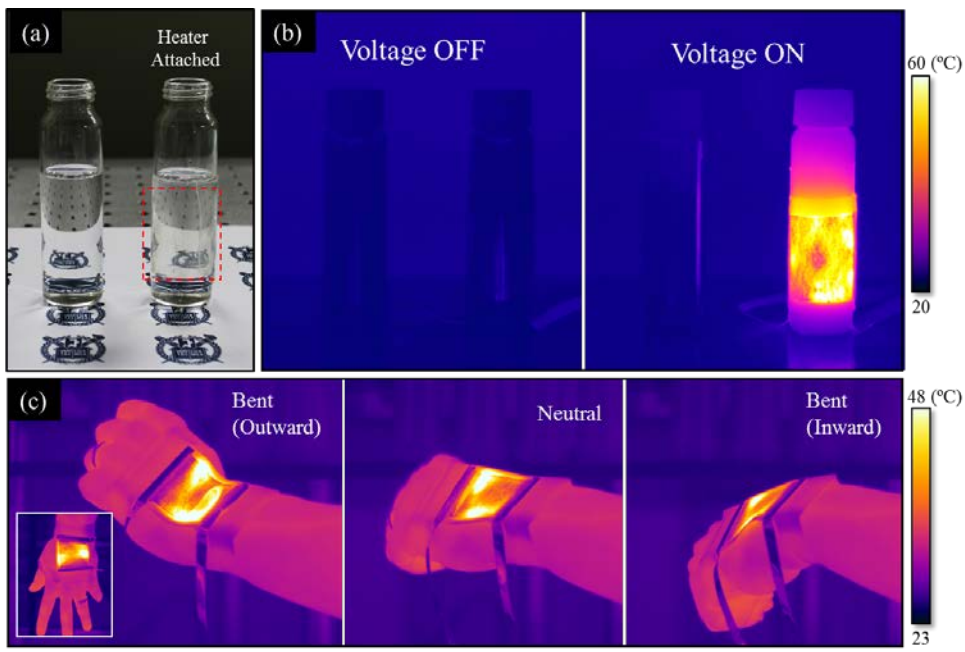

Figure 34. a), Image of STSN heater attached to a glass vial (Red dotted line). b), Temperature distribution image of two glass vials before applying DC voltage (Left) and after applying DC voltage (Right). c), Temperature distribution image of stretchable and transparent heater affixed to a human wrist at outward bending (Left), neutral (Center) and inward bending (Right) conditions. Inset is a temperature image captured from different angle.

As the underlying PDMS is bendable, lightweight and cohesive, the entire heater can be easily attached to a bent surface with good conformal coverage. In Figure 35, one of two glass vials filled with DI water is wrapped with the Ag NW network electrode at the bending radius r=15 mm in the red dotted area. It is observable that the vial still preserves optical transparency with the heater attached. Upon the application of a DC voltage, heat dissipated from the STAN heater is efficiently transferred to the water inside through the vial as in Figure 35 (b) since the heater is attached conformably to the glass vial. As a result, the water inside the glass vial is heated up using much less energy compared to a rigid heater. Note the temperature difference between the vial and ambient even after the heating, which verifies the temperature increase of the target water in the vial. Another advantage of PDMS comes from its bio-compatibility, as previous studies on PDMS have reported that it is not expected to cause any significant irritation or other adverse effects on human skin and the immune system. The STSN heater is directly affixed to the human wrist in order to examine its operation at various physical disturbances including bending, stretching and twisting which are commonly involved in general human motions. Figure 35 (c) shows some representative temperature profiles captured at elevated temperatures for three different conditions of inward bending, outward bending and neutral state, which proves that the resultant heater exhibits fine performance with high stability at mechanical disturbances including compressive and tensile strains.

In conclusion, the results presented herein demonstrate that the Ag NW network / PDMS electrode prepared exhibits good electrical conductance at high optical transmittance with superior mechanical, electrical and thermal stability to enable a stretchable and transparent heater for future wearable electronics applications. Due to its unique interfacial morphology, the STSN heater operates successfully operates under both elevated temperature (60 ℃) and large strain (60 %) with excellent reliability. At the same time, the respective merits of PDMS and Ag NW are still preserved. Moreover, as these constituents are well known, widely studied and solution processable with facile procedures, we expect that the resultant Ag NW / PDMS has high availability and scalability for future wearable applications.

Chapter 4. Fabrication of transparent and stretchable supercapacitor using Au-Ag core shell nanowire

4.1. Au-Ag core shell nanowire

Supercapacitors, owing to long cycle life with rapid charging and discharging capabilities at high power density, have long become a most viable candidate to substitute conventional batteries. Recently, the interest towards supercapacitors is ever-growing, especially for those on non-rigid substrates[17, 18], due to the rapid increase in demand for portable and wearable electronics. Since these devices are intended to be attached to the human body and operated under continuous mechanical disturbances such as bending, twisting and stretching, supercapacitor has huge benefits over conventional batteries for their associated energy device in terms of portability and safety, having lighter weight as well as lower risk of explosion.[45] On the other hand, the latest progress on the development of next generation future electronic devices in both industry and academia[46, 47] further suggests that the ultimate form of supercapacitor should not only be stretchable, but going another step forward to be optically transparent[48] in order to achieve additional versatility and support easy integration with other wearable devices. To these objectives, there have been some attempts to fabricate a stretchable and transparent supercapacitor based on carbon based nano materials including CNT and graphene.[46, 49-51] However, these materials typically require additional schemes on the target substrates such as employing wrinkles or applying pre-strain to attain meaningful

stretchability over the device. These supercapacitors which depend on the pre-treated substrates are difficult to be integrated into a stretchable electronic circuit. Moreover, these CNT or graphene based transparent electrodes generally suffer from high electrical resistance due to the inherent defects in the pristine materials or derived from the fabrication process.[23, 52] For the high performance stretchable and transparent supercapacitor, a novel conductive platform that possesses superior electrical conductivity together with good optical transparency and mechanical stretchability at the same time is therefore in need.

In this regard, Ag NW percolation network can be an excellent candidate as a platform for the stretchable and transparent supercapacitor. Ag NW percolation network has been intensively studied and become a markedly mature technology as a novel transparent conductor to replace Indium-Tin-Oxide (ITO),[53] and its application has been successfully extended to stretchable and transparent electrodes to withstand repeated external strain.[54] However, despite these advantages, its poor electrochemical stability has forbidden the use of Ag NW percolation network as a main material for wearable electrochemical energy devices including supercapacitor. Upon the application, the electrolyte in the supercapacitor dissolves the Ag NW through ionization, and the performance of the resultant supercapacitor with Ag NW network electrode deteriorates rapidly at typical operating voltage range.[55] In order to overcome this problem and develop the next-generation platform for a stretchable and transparent supercapacitor, the electrochemical stability of the Ag NW percolation network has to be enhanced in an essential respect.

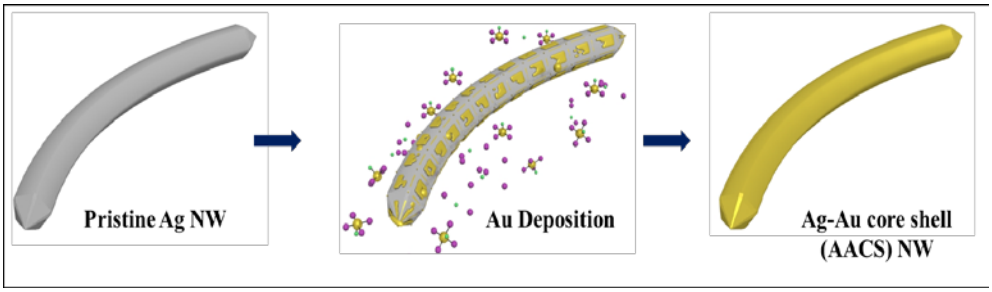

Figure 35. Schematic illustration of AACS nanowire fabrication.

In this study, as shown in Figure 35, we introduce electrochemically stable Ag–Au core shell (AACS) NW network with high stretchability and transparency for wearable energy device application. AACS NW, synthesized through a simple Au coating process in solution environment, is composed of the core Ag NW with a thin gold outer layer at nanoscale. Although the consumption of high-priced Au in preparing AACS NW is minimized compared to the synthesis of an ordinary Au NW, it is confirmed that the outer Au layer on AACS NW strikingly improves the chemical and electrochemical stability of the overall AACS NW. At the same time, the theories, processes and practices developed for conventional Ag NW are directly applicable to the AACS NW to readily create AACS NW percolation network for highly stretchable and transparent electrode.

4.2. Synthesis of Au-Ag core shell nanowire

We developed the electrochemically more stable sheath forming method around the original Ag NW through the facile solution process. The surface of the Ag NW is coated with Au atoms through reduction of Au ions as schematically illustrated in Figure 35. The pristine Ag NWs are introduced into aqueous solution which contain capping agent, reducing agent and pH increasing agent, followed by the slow injection of Au precursor through motorized syringe pump. The detailed experimental conditions are as follows.

Preparation of AACS NW:

a) 1 mM aqueous solution (20 mL) of PVP (MW: 55,000, Sigma Aldrich) is poured into 50 mL Erlenmeyer flask with an elliptical stirrer.

b) 0.1 M aqueous solution (5 mL) of AA (L-Ascorbic acid, FW: 176.12, Sigma Aldrich) and 0.2 M aqueous solution (5 mL) of NaOH (Sigma Aldrich) are injected into the PVP solution sequentially, keeping the stirrer vigorously rotating.

c) After the mixture becomes a clear solution, 100 μL of 0.5 wt% Ag NW aqueous solution (NW Diameter: 30 nm~35 nm, N&B Co.) is added into the reaction solution.

d) As the final additives, 0.15 mM aqueous solution (6 mL or 12 mL for thin or thick Au layer) of HAuCl4 (FW: 339.79, Sigma Aldrich) is injected into the reaction solution through motorized syringe pump at 45 μL/min injection speed.

e) After all the Au precursor is injected, the Ag-Au core shell NWs are separated and washed by DI water for three times through centrifugation.

f) The separated Ag-Au core shell NWs are kept in mixture of DI water and ethanol. (2 mL DI water, 18 mL ethanol) in conical tube.

During this process, the key factors for conformal coating of Au atoms on the Ag NW surface are adequate pH of the reaction solution and the injection speed of the Au precursor. Failure in satisfying either condition results in porous Au nanotubes as shown in Figure 36 since those factors are crucial for blocking the galvanic reaction that causes the loss of Ag atoms from Ag NW.[56, 57] Au outer shell is successfully created on the surface of Ag NW at high conformity once these conditions are satisfied simultaneously. In adequately high pH solution, the reduction power of reducing agent is optimized to prevent the Au precursor involving in galvanic reaction with Ag NW[57]. At the same time, as the Au precursor is injected very slowly, the Au atoms derived from the precursor do not nucleate themselves, but epitaxially deposit on the surface of Ag NW in the reaction solution under vigorous stirring.

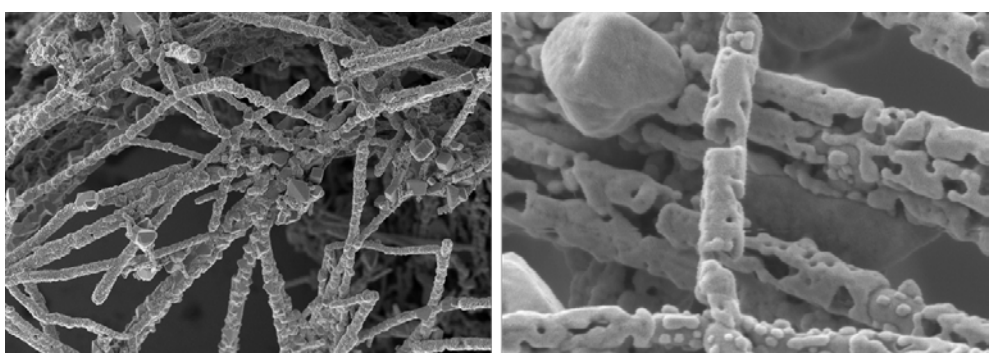

Figure 36. Synthesis results of AACS NW at unoptimized conditions.

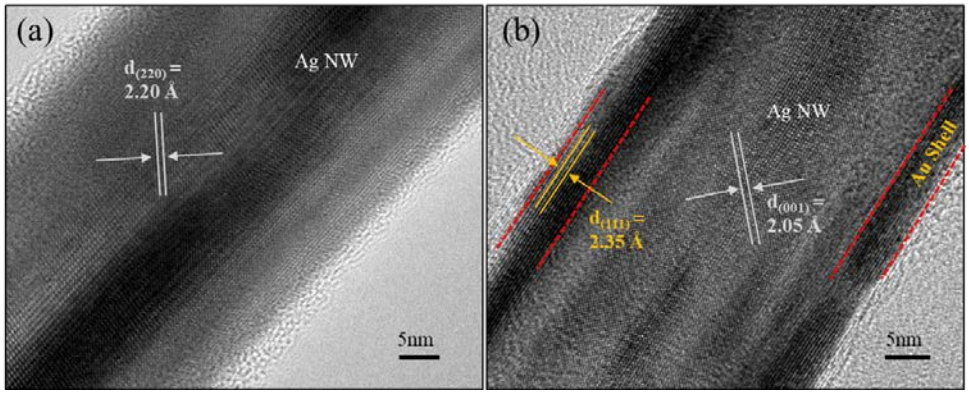

Figure 37. TEM images of (a) Ag NW and (b) AACS NW with crystalline analysis.

Figure 37(a) shows TEM image of the pristine Ag NW. The lattice distance of 2.20 Å measured from the image processing reveals that the periodic structure observed in the image corresponds to [220] direction of single crystalline Ag.[58] After a complete coating process, AACS NW is obtained as shown in the TEM image in Figure 37(b). The clear contrast change from light to dark in both sides signifies that there are heavy atoms as compared with the core region. More close examination on the outer region clarifies that the periodic structure matches to [111] direction of single crystalline Au.[59] Having the core Ag NW remains unchanged, superior electrical conductivity as well as the mechanical robustness of the primary NW are expected to be preserved during the Au deposition process.

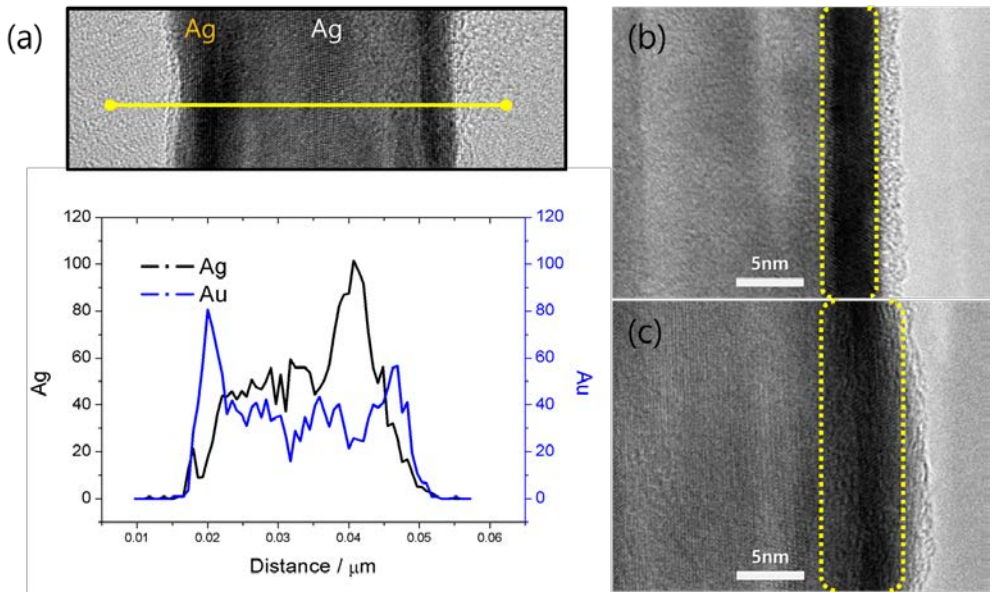

Figure 38. a) TEM-EDX line profile of the AACS NW, b), c) Thickness variation of Au shell layer depending on the Au precursor amount.

TEM-EDX line profile in Figure 38(a) further proves that the final product is indeed AACS NW which is composed of core Ag NW of ~30 nm diameter with Au shell at ~5 nm thickness. The line EDX profile measured following the yellow line of the TEM image shows that the dark contrast at both edges is resulted from Au layer on the Ag NW surface. Naturally, the thickness of Au shell layer can be easily controlled by changing the amount of the injected Au precursor as verified in Figure 38(b) and (c). Except for the amount of the injected precursor solution, all the other experimental conditions are same in both (b) thin and (c) thick cases. 6mL and 12mL of 0.15 mM $HAuCl_4$ solution are used, respectively.

To provide evidences of galvanic replacement-free deposition of Au on Ag NW, as galvanic process causing the destruction of Au NW is mostly spontaneous, average diameter changes of nanowire measured and calculated from multiple SEM images before and after the ~3nm Au layer deposition process. The thickness of the deposited Au layer is well matched with the half of the average NW diameter increase (~2.75 nm) after the Au deposition process as shown in Figure 39. Therefore, it is worth mentioning that the proposed Au coating process does not involve any replacement of Ag atoms upon the reduction process implying that the reaction is largely galvanic replacement free.

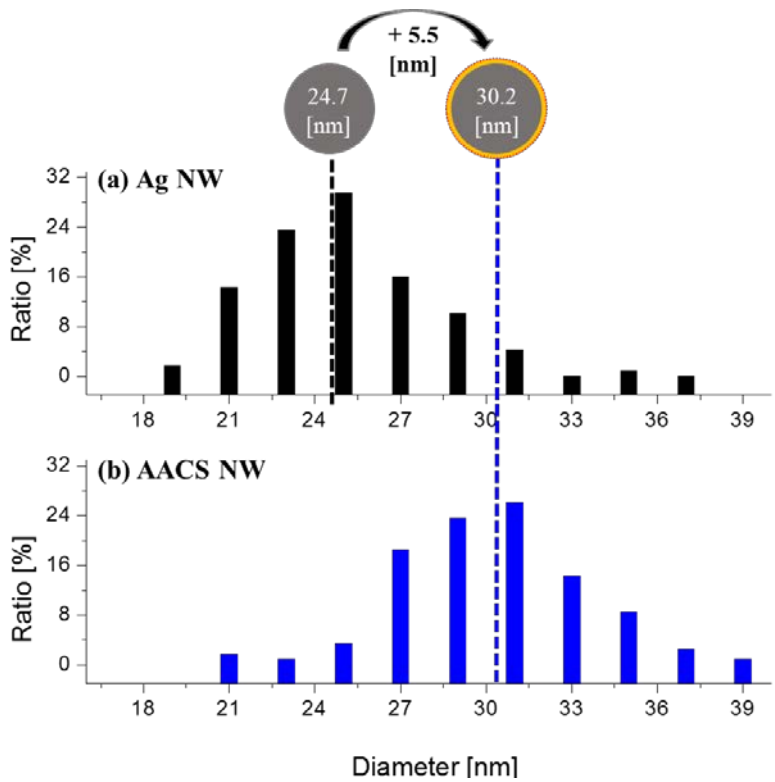

Figure 39. Average diameter changes during the Au deposition process.

4.3. AACS NW percolation network electrode

With the developed AACS NWs, the theories and technics of Ag NW ascribed before can be used to create NW network based transparent and stretchable electrodes. The vacuum filtration and transfer method is used again this study to prepare the highly stretchable and transparent AACS NW network electrodes and the procedure is schematically illustrated in Figure 40. For a typical preparation, AACS NW solution is poured into the filtration cup which is connected tightly with PTFE filter and after complete filtration of the solution the resultant AACS NW network on the filter is transferred to the target substrates. Depending on the target substrates, just transparent electrodes or transparent and stretchable electrodes can be prepared.

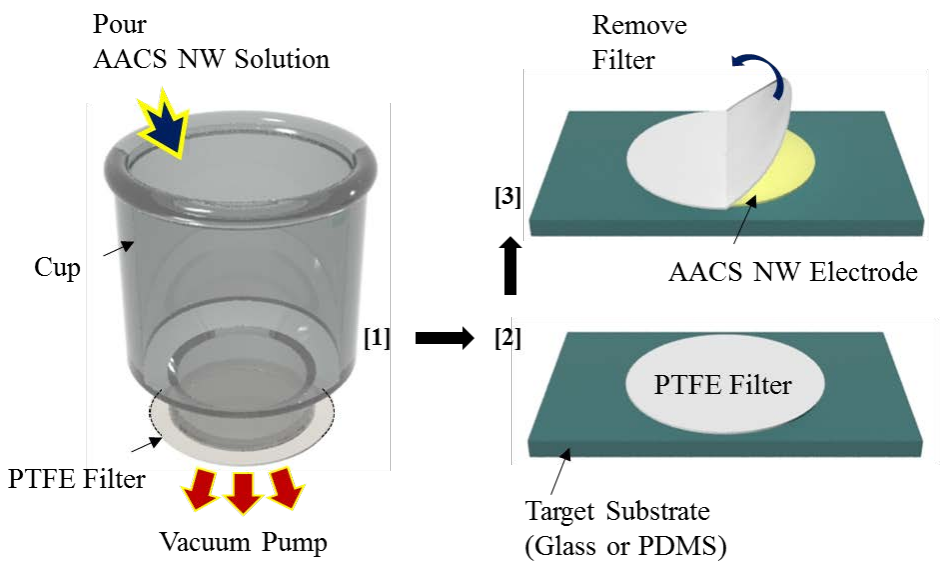

Figure 40. Schematic illustration of the AACS NW electrode fabrication through vacuum filtration and transfer method.

Figure 41(a) shows the AACS NW network / glass electrodes with various sheet resistances from 42.3 Ω/sq to 167.7 Ω/sq depending on the density of AACS NW. Figure 41(b) showing the results of UV-VIS spectrometer measurement confirms that the AACS NW networks possess superior optical transparency, exceeding 85 % in the entire range of visible wavelength. The areal density of AACS NW corresponding to each electrodes is calculated and the results range from 52 mg/m2 to 268 mg/m2. It is noticeable that the prepared AACS NW electrodes are comparative to the Ag NW based electrode in terms of both the transparency and the sheet resistance.

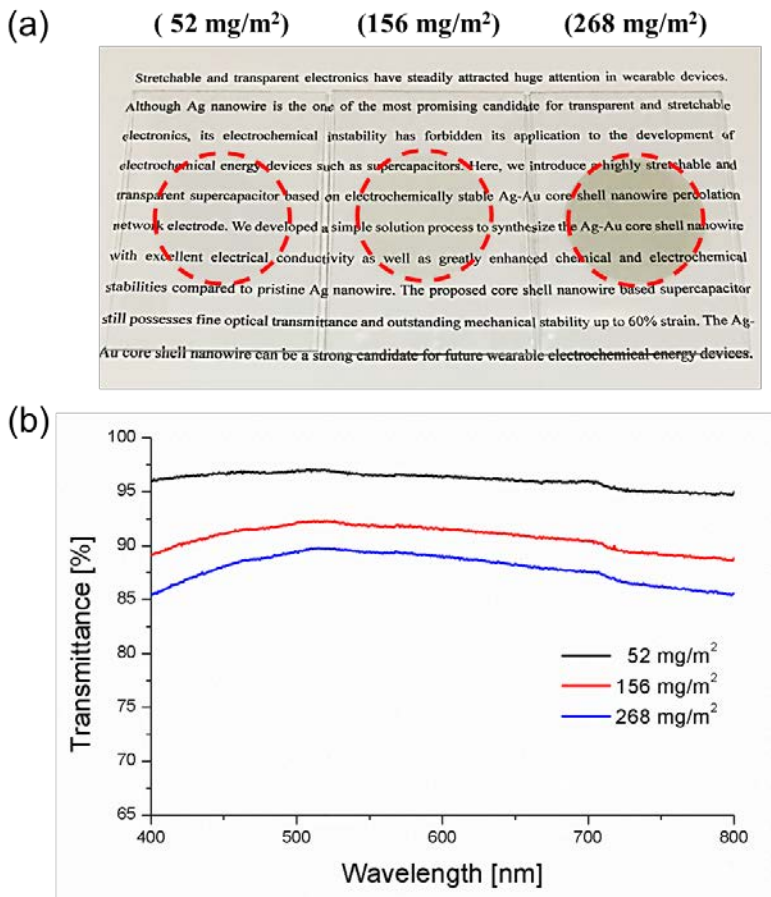

Figure 41. a) Photographs of transparent AACS NW electrodes at various NW density, b) Optical transmittance of the transparent electrodes.

We have demonstrated before that when Ag NW network is deposited on the PDMS substrate, the transparent electrode can sustain its electrical conductivity under a large strain due to the unique structural features of NW percolation network / PDMS composite. Herein synthesized AACS NW can be likewise applied as a constituent of transparent and stretchable electrode on PDMS substrate. Subsequently, the AACS NW based stretchable and transparent electrode is prepared and its stretchability is analyzed through measuring the electrical resistance change in stepwise strain variation. The result is summarized in Figure 42 with an inset image which shows the experimental setup consisting of the AACS NW / PDMS electrode with both ends connected to copper tape on the horizontally moving stage.

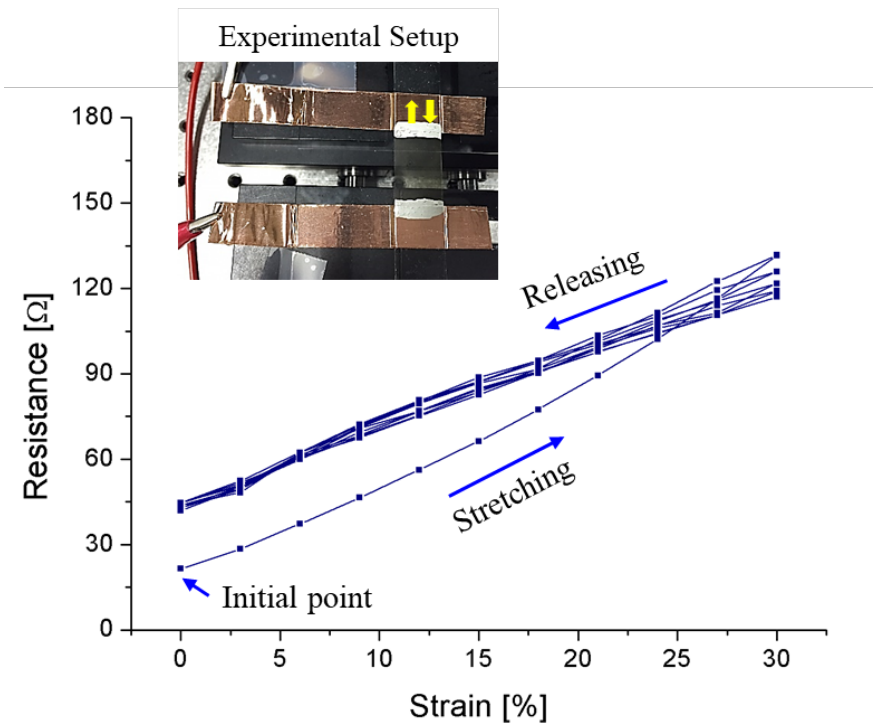

Figure 42. Strain-dependent electrical resistance variation of AACS NW / PDMS electrode.

It is well-known that metal NWs such as Ag NW, those with smaller diameter in particular, have degrading stability problem to lose their electrical conductivity even in ambient condition. Being an inert noble metal with high reduction potential compared to Ag, Au sheath created around the surface of Ag is expected to increase the overall stability of the electrode to the environment. For comparison, three types of electrodes (pristine Ag NW, AACS NW with thin and thick Au sheath layers) are prepared at 2x2 cm^2 size and their electrical resistance variation over time is monitored. These electrodes are placed in controlled environment maintaining temperature of 22°C and relative humidity of 45% to mimic the ambient condition.

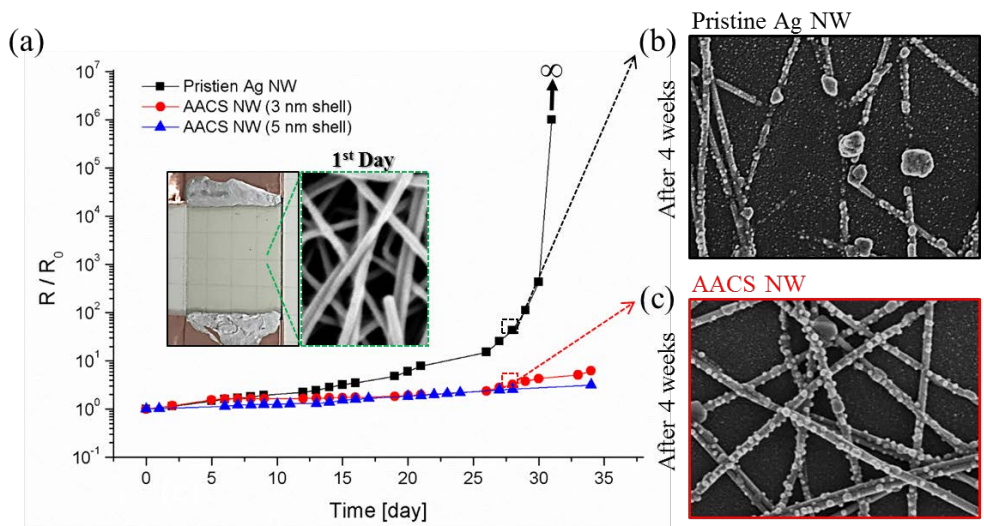

Figure 43. Aging test of Ag NW and AACS NW electrodes under ambient condition.

As can be seen in the inset of Figure 43(a), the surface of NW of is smooth without any residue except NW, yet the resistances of the electrodes increase gradually over time and it is noticeable that pristine Ag NW electrode (black line) degrades

much faster than AACS NW electrodes (blue and triangle lines). It is apparent from Figure 43(b) that the surface of the Ag NW is covered with tiny nanoparticles after 4 weeks, and most of the NWs are disconnected to show electrical failure. In contrast, although similar small nanoparticles are observable on the surface, AACS NW network almost maintain their overall structure as close to its original state for both cases of thin and thick Au layer coating (Figure 43(c)). The electrical measurements in Figure 43(a) are also consistent with the SEM images, confirming the enhancement of electrode stability in ambient condition by Au coating on the Ag NW surface.

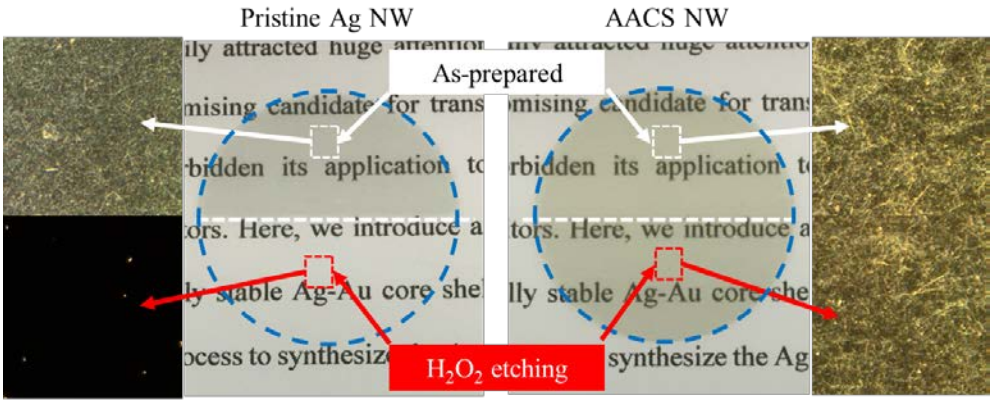

Figure 44. Digital and optical microscope images of Ag NW (left) and AACS NW (right) electrodes after H_2O_2 corrosion test.

Enhancement in chemical stability of the AACS NW owing to Au outer shell is valid even in the liquid chemicals which is much harsh condition than the ambient environment. As an extreme example, H2O2 etching test are conducted on the Ag NW and AACS NW network electrode. As it is well known that the H_2O_2 chemically

dissolve the silver very efficiently, this test could show the protecting performance of Au shell. Ag NWs and AACS NWs electrodes are prepared at high densities, and the half of each electrode is immersed in 12.5 % H_2O_2 aqueous solution for 1 minutes, followed by DI water cleaning. The photographs and corresponding optical microscope images of the electrodes before and after the etching test are displayed in Figure 44. After the short contact with H_2O_2 solution, the Ag NWs (left pictures) are immediately degraded with a large amount of bubbles generation and the immersed Ag NWs are mostly removed from the glass substrate. In contrast, for the AACS NW electrode (right pictures), there is no perceptible change as presented in the photograph and even optical microscope images. This result implies that the Au shell layer successfully protect the core Ag NW against the attack of the corrosive chemicals and therefore make the NW network electrode maintain its performance even at such harsh condition in which the Ag NWs are dissolved instantly.

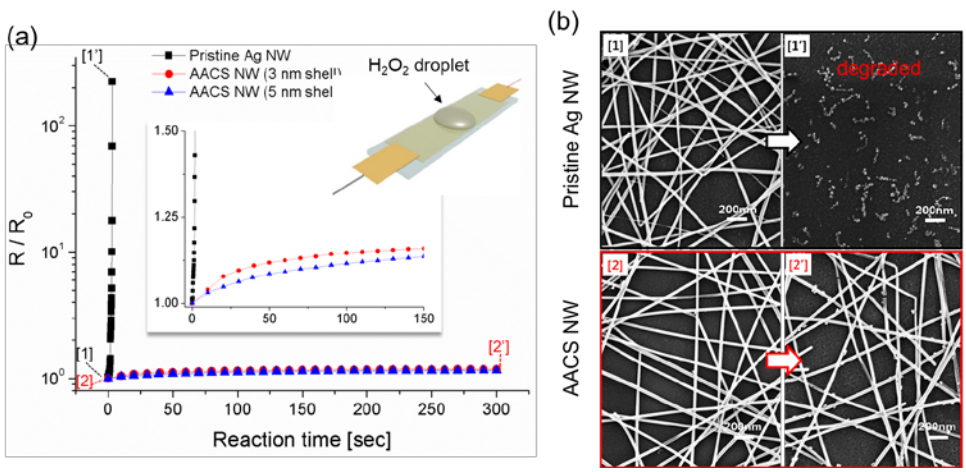

Figure 45. a) Electrical resistance changes under H_2O_2 exposure. Insets are an enlarged graph and schematic experimental setup. b) SEM images of pristine Ag NW (top row) and AACS NW (bottom row) before and after he corrosion test.

The electrical resistance change upon the exposure to H_2O_2 solution also confirms the advantage of Au coating as shown in Figure 45(a). The inset shows the same graph with enlarged y-axis and from the graph it is noticeable that there is a minute change of the electrical resistance in both thin (red line) and thick (blue line) AACS NW electrodes. Figure 45(b) shows the SEM images of the electrodes after the chemical corrosion test. The pristine Ag NWs (top row) are totally dissolved and only negligible residue is found. On the other hands, the AACS NW electrode (bottom row) shows insignificant change in its feature, but with some tiny particles sparsely attached on the surface. It can be estimated that there are some fine pores or defects on the Au layer and therefore a small fraction of the core Ag NW is exposed to the H2O2 solution and generate tiny particles similar to the ones shown in top right of Figure 45(b). These partial damages are also consistent with the resistance transient change which indicates an initial slight increase in the electrical resistance of AACS NW. Yet, increase in resistance is infinitesimally small, especially for the one with thicker Au shell (blue line), compared to the dramatic resistance upsurge in pristine Ag NW network (black line). These results clearly validate that the core Ag NW is well protected by the Au shell to achieve highly enhanced chemical stability.

4.4. Transparent and stretchable supercapacitor

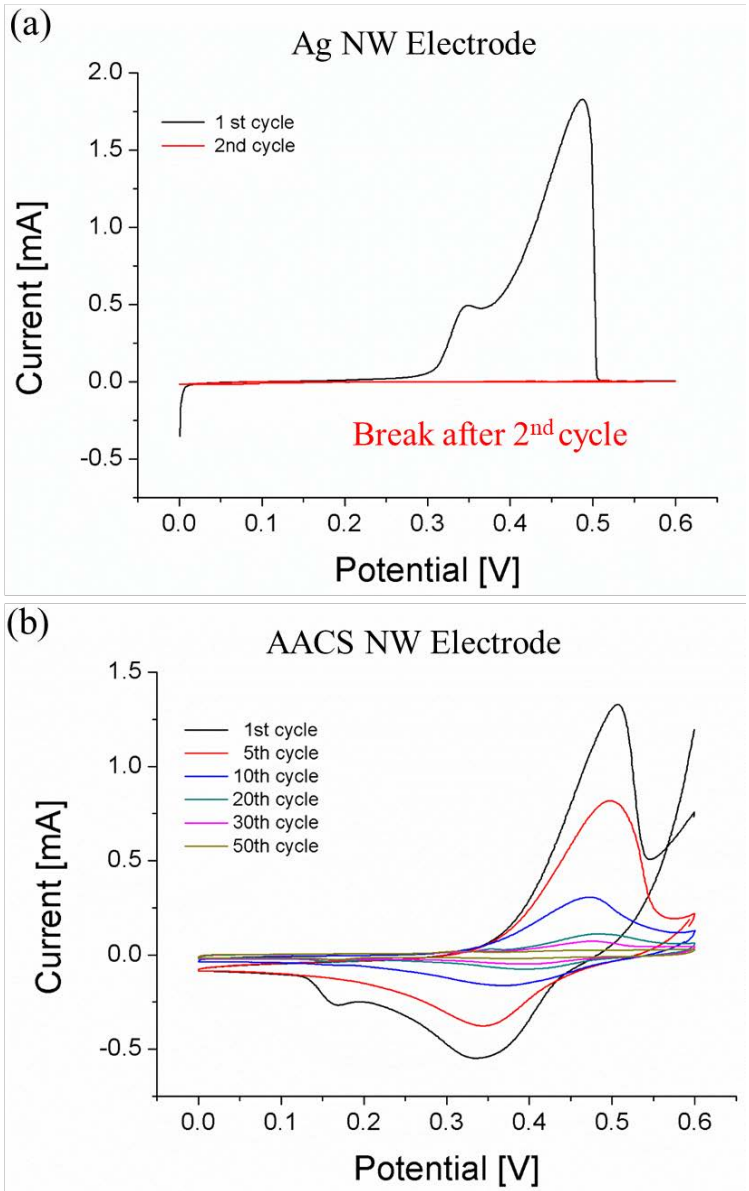

Figure 46. CV curves of Ag NW and AACS NW electrode as electro chemical stability test.

Even though the AACS NW electrode shows improved stability in ambient condition and harsh chemical solution, the electrochemical stability is essential for energy device to sustain its performance under the applied voltage. To examine the

electrochemical stability of the resultant AACS NW electrode, cyclic voltammetry (CV) test is conducted. A typical three-electrode measurement method is used with Ag/AgCl reference electrode and Pt counter electrode in the Na_2SO_4 aqueous electrolyte. The CV test result for the pristine Ag NW electrode shows an oxidation peak at the 1^{st} cycle followed by rapid current drop and flatten curve without corresponding reduction peak at the reverse voltage scan region as displayed in Figure 46 (a). The potential value at the peak corresponds to the characteristic oxidation peak of typical Ag. This signifies that an irreversible reaction is occurred in the electrode material during the 1^{st} oxidation and the Ag ions are dissolved directly into the electrolyte solution. In contrast, CV result of AACS NW electrode shows typical CV curves as displayed in Figure 46 (b). Oxidation peaks are also found at ~ 0.45 V potential value which is the same as the oxidation peak of Ag NW electrode, however, there are corresponding reduction peaks at the reverse voltage scan state in every CV cycles without rapid drop of the current. As the AACS NW possesses tiny defects or pores in the Au surface, the core Ag NWs are partially exposed to electrolyte and the Ag ions are generated only at the exposed spots. Since the Ag ions are largely protected by the Au shells, they mostly do not dissolve into the electrolyte nor diffuse away from the electrode. As a result, these Ag ions in the vicinity of Au shell are likely to involve in the reduction procedure and generate reduction peak in the CV curve during the reverse voltage scan. It is also observable that those peaks diminish as the cycles continues, and the CV curves eventually converge to rectangular shape after 50 cycles.

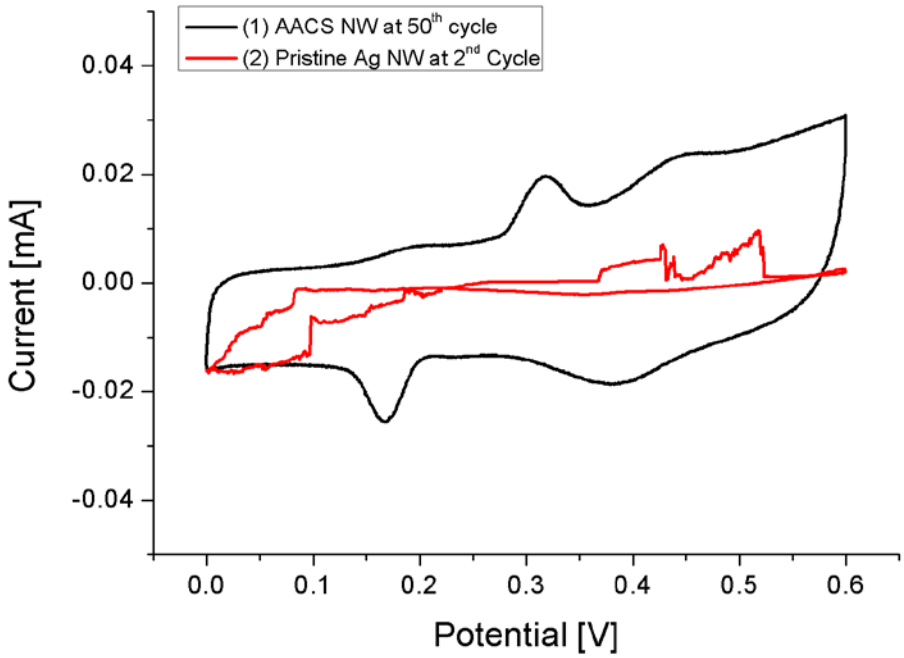

Figure 47. CV curves of Ag NW and AACS NW electrode.

The stabilized CV curve of AACS NW electrode is included in Figure 47, drawn simultaneously with the 2nd CV cycle of Ag NW electrode. There is a pair of peaks which are produced at different potential values with Ag. These peaks indicate the properties of Au and it signifies that there are no more Ag atoms which are actively involved in the CV test.

Through successful realization of novel class of metal NW which possesses highly improved electrochemical stability, stretchable and transparent supercapacitor composed of AACS NW percolation network is demonstrated for wearable electronics applications. The detailed process is as follow with Figure 48.

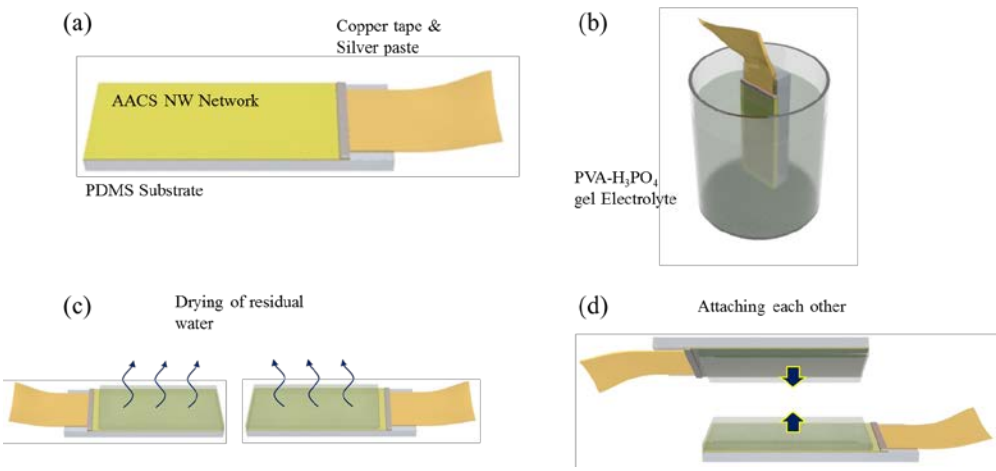

Figure 48. Fabrication process of all solid-state supercapacitor using AACS NW electrode.

(a) The AACS NW based electrode is cut into 1 cm x 2 cm square and one side of the electrode is connected to copper tape with silver paste.

(b) The electrode is immersed in polymer electrolyte solution for 1 minute except the copper tape.

(c) A pair of electrode are kept in fume hood for 4 hours after the electrolyte deposit process to dry the residual water of the electrolyte layer. In this step, the electrolyte gel layer changes to colorless transparent polymer film.

(d) Two identical electrodes are attached together by the solidified electrolyte film acting as a glue. Mild pressure is applied on the both sides for another 1 minute.

In the proposed supercapacitor, AACS NW electrode acts as both active material and current collector, while the H3PO4 polymer gel acts as both separator and electrolyte. Unlike the result of three electrode CV test in aqueous solution (half-cell test), the CV test of full-cell which is assembled by the gel electrolyte with two identical AACS NW network electrodes shows neither oxidation nor reduction peaks as shown in graph of Figure 49. The photograph shows the transparent AACS NW based supercapacitor.

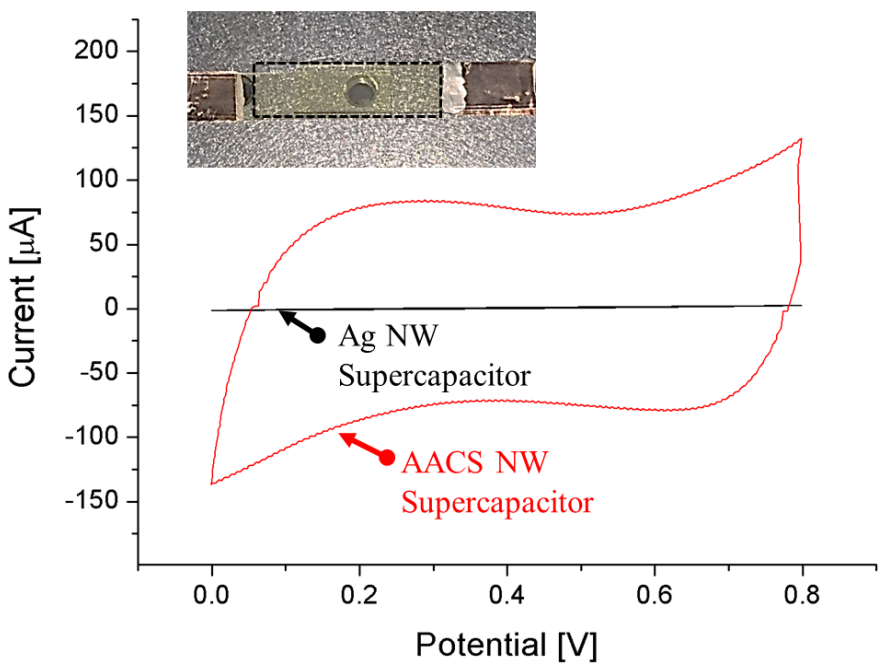

Figure 49. Comparison of CV curves between Ag NW based supercapacitor and AACS NW based supercapacitor.

Before, it is confirmed that oxidation and reduction peaks of AACS NW are originated from the dissolution of the inner Ag NW into liquid electrolyte through the tiny defects or pores of the Au

shell. Different from liquid electrolyte, the polymer gel electrolyte cannot penetrate into the tiny pores of Au shell due to its high viscosity, solid like properties. As a result, the Au shell layer keeps the Ag core NW from contacting with the polymer electrolyte, and therefore the effect of the polymer electrolyte, which is to dissolve Ag atoms in contact, is almost insignificant. The benefit of employing AACS NW as the electrode of the supercapacitor is clearly observable from the CV curve of an Ag NW based supercapacitor whose result is drawn simultaneously as black line in Figure 49.

Furthermore, to observe the mechanical stability of the AACS NW based transparent and stretchable supercapacitor, CV test is performed at various voltage scan rate under increasing strain condition. As a result, the AACS NW supercapacitor not only exhibit optical transparency, but also sustain its performance in a very large strain condition as presented in the Figure 55. The CV curve slightly increases along with the strain up to 30% and this trend could be explained by decrease in the gap between upper and lower electrode together with the enlarged working area.[60] It is noticeable that the shape of CV curve slightly changes at 60% strain, especially in the fast voltage scan condition. The deformation of the CV curve under high strain and fast voltage scan condition might be derived from the temporary electrode resistance increase which is recovered after strain releasing

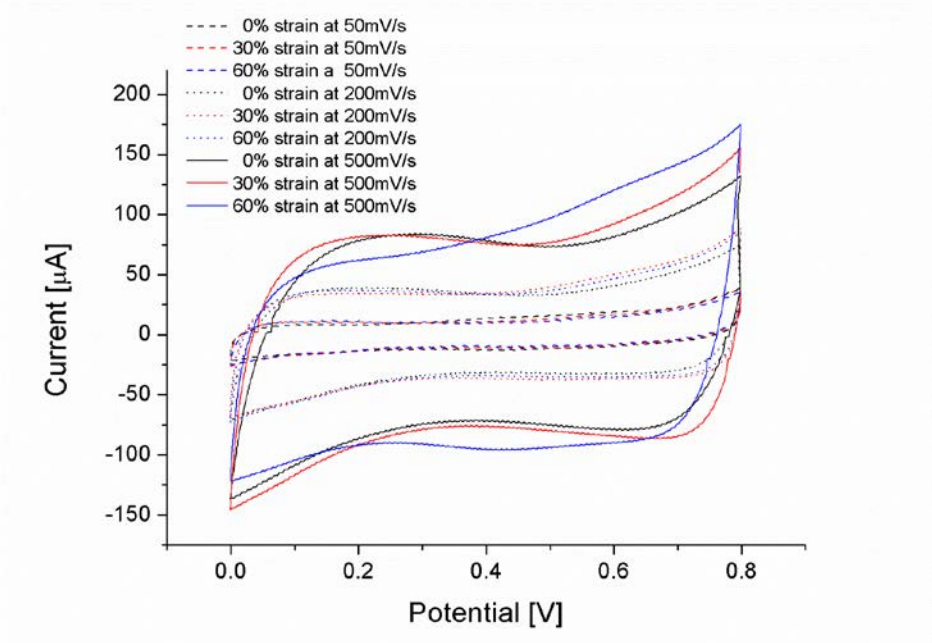

Figure 50. CV curves of AACS NW supercapacitor at various strain condition (0 %, 30 %, 60 %) and voltage scan rate (50 mV/s, 200 mV/s, 500 mV/s).

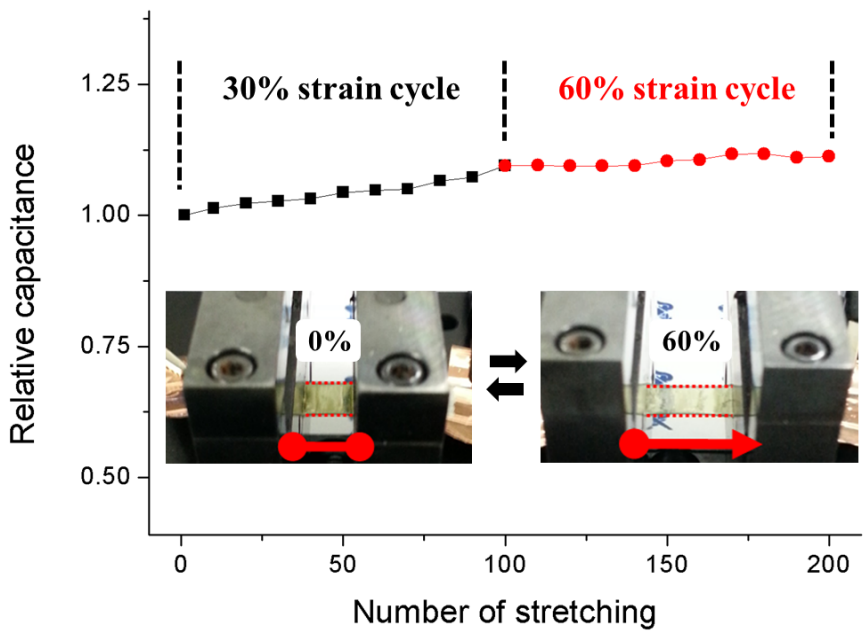

Figure 51. The relative capacitance change of the AACS NW supercapacitor during the repeated stretching cycles.

Also, the supercapacitor sustains its electrochemical performance even after the 200 times stretching cycles as shown in Figure 51. First 100 cycles are conducted under 30% strain condition and the other 100 cycles are conducted under 60% strain condition. The insets are digital images of AACS NW supercapacitor at 0% and 60% strain condition.

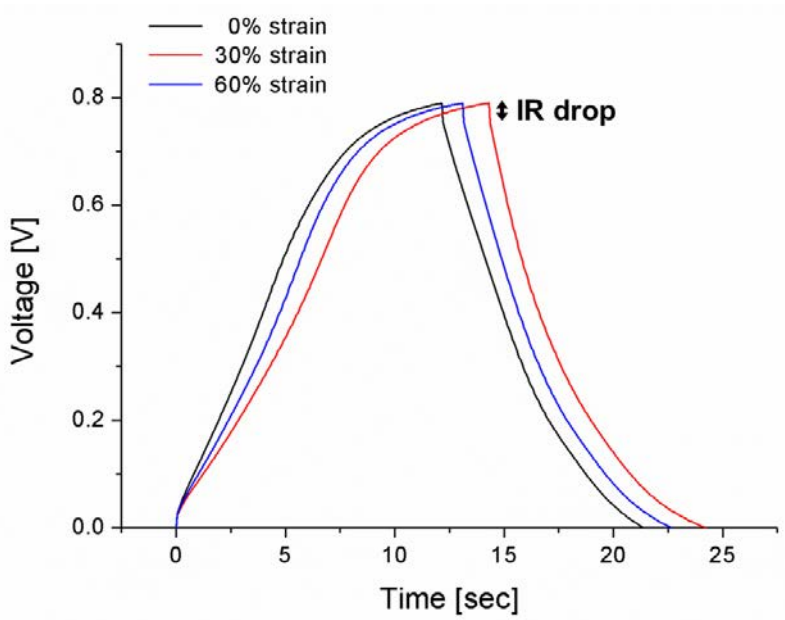

Figure 52. The Galvano-static charge-discharge curve of AACS NW supercapacitor under various strain condition (0 %, 30 %, 60 %).

The charge-discharge curves under different strain condition indicate, once again, the good capacitive properties with high mechanical stability of the resultant supercapacitor. The curves sustain their triangular shape with unremarkable IR drop under increasing strain condition up to 60 %. Considering that the required strain range of wearable devices is about 55%, these results are very encouraging for applying the prepared stretchable and transparent supercapacitors as an energy source for various fully stretchable wearable device.

Additionally, three AACS NW supercapacitors are connected in series to turn on a red-LED as shown in Figure 53(a) and the CV curve for the series connected supercapacitors is attached in Figure 53(b). The series connected supercapactiors are successfully charged and discharged lighting on the red-LED even at 30% strain condition. To the best of authors' knowledge, this is the very first example of operating a commercial electronic device with a stretchable and transparent supercapacitor at its stretched state.

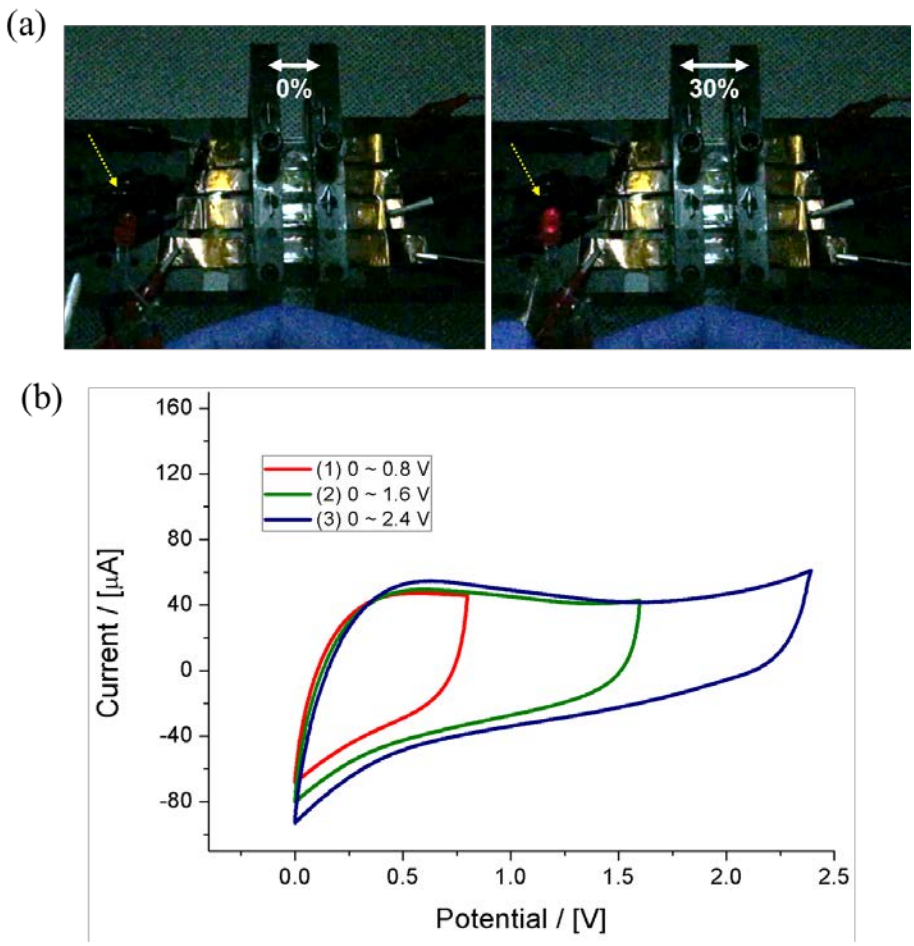

Figure 53. Operating of series connected AACS NW supercapacitor with corresponding CV curves.

4.5. Increase the capacitance of the supercapacitor

In an effort to realize supercapacitor having higher energy storage performance for wearable electronics application, we suggest a direct electro-polymerization of conducting polymer method on a metal nanowire network by using AACS NW to achieve an Ag/Au/conducting polymer core-shell NW. In this research phase, we used polypyrrole (PPy) as an active polymer layer considering its superior thermal stability, fast charge-discharge mechanism, and mild electro-polymerization condition.[61-65] Since the standard reduction potential of gold (+1.50 V) is higher than monomer of conducting polymer (e.g., Pyrrole, +0.8 V) [66] AACS NW can successfully undergo the electro-polymerization process, resulting in an Ag/Au/conducting polymer core-shell NW mesh without damaging the original nanowire. Figure 54 shows the whole fabrication process of Ag/Au/PPy core-shell NW (AAP NW) network based electrode.

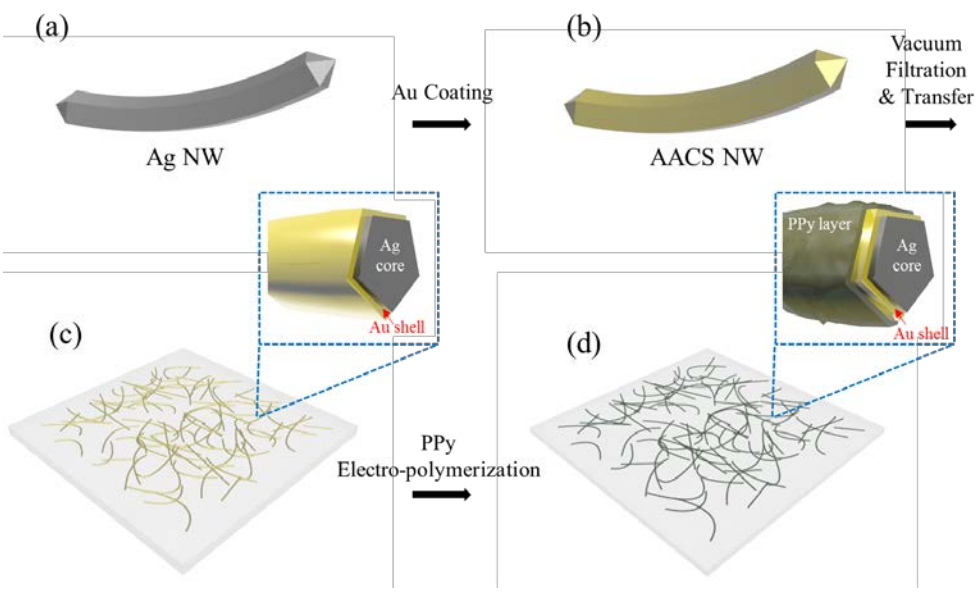

Figure 54. Fabrication step of AAP NW network electrode

This process includes three simple steps. First, pristine Ag NWs with a diameter of 30 nm are coated with a thin gold layer through earlier mentioned method in chapter 4.2. Subsequently, AACS NWs dispersed in ethanol are transferred onto a polyethylene terephthalate (PET) substrate through the vacuum filtration and transfer method, which results in a well-connected nanowire percolation network with high electrical conductivity as well as optical transparency. In this work, the density of AACS NW is fixed to 12.5 $\mu g/cm^2$ which guarantees both electrical conductivity and transparency of the NW based electrode. After that, the AACS NW network electrode is immersed in pyrrole-dissolved solution for electrical coating of PPy through cyclic potential sweep. In this study, all of the electro-polymerization processes are conducted under the same condition (a scan rate of 0.2 V/sec ranging from 0 to 1.0 V) except for the number of voltage sweep cycles to control the thickness of the PPy layer.

To confirm the synthesized AAP NW network structure, we performed a focused ion beam (FIB) cross sectional imaging analysis on the fabricated mesh film that underwent 15 cycles of PPy coating cycle. As shown in Figure 55(a), the PPy is conformally coated on the AACS NW surfaces and the diameter of the resulting AAP NW is approximately 100 nm. As shown in Figure 60(b), FIB analysis revealed the existence of core Ag (grey pseudo-colored) without any observable damage, even after the electro-polymerization process, while the PPy polymer shell (cyan pseudo-colored) is coated uniformly over the AACS NW network. The core-shell structure is more closely examined with a transmission electron microscopy (TEM) analysis. The specimen for TEM analysis is prepared by scraping out the AAP NWs on the

glass substrate and directly attaching them on the holey carbon grid. Figure 55 (c) shows the TEM image of the AAP NW structure. The periodic lattice distance of 2.05 Å and 2.35 Å corresponds to [001] direction of single crystalline Ag and [111] direction of single crystalline Au respectively. PPy layer on the Au shows amorphous structure from the TEM image.

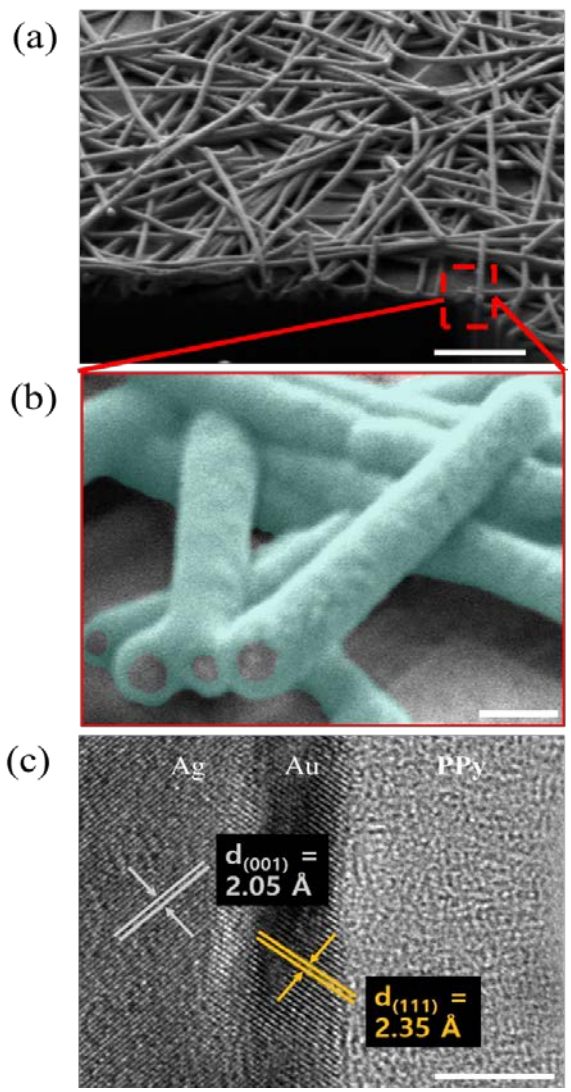

Figure 55. Sturcture analysis of AAP NW, a,b) FIB-SEM image of AAP NW on PET substrate, c) High resolution TEM image of core-shell structure. Scale bars in (a), (b) and (c) show 1 μm, 100 nm, and 5 nm respectively. Sturcture analysis of AAP NW.

As the Ppy polymerization directly depends on the total charges participated in the electro-polymerization process the amount of Ppy, which would be the key factor of the energy density of the supercapacitor, can be controlled by the coating cycles. Also, since the thickness of Ppy layer coated on the AACS NW surface affects to the transparency of the electrode as well, an appropriate amount of Ppy should be selected.

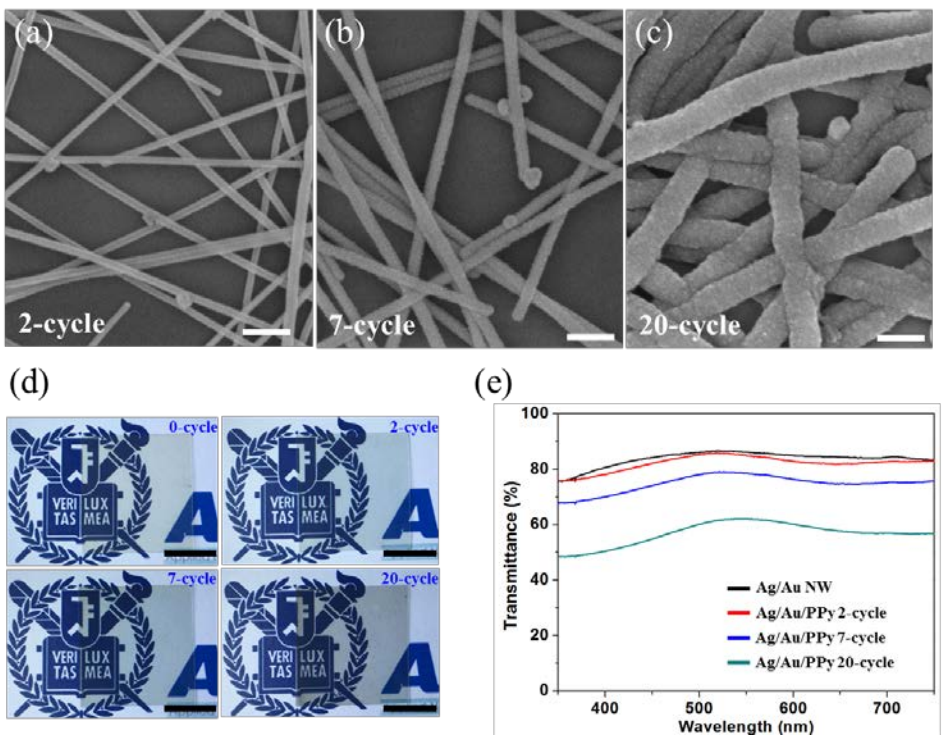

Figure 56. SEM and optical image of AAP NW electrode fabricated through various Ppy coating cycles and their transmittance.

In this regards, AAP NW network electrode on PET films are fabricated through various number of coating cycles from 2 to 20. Figures 56 (a-c) show the SEM images of the AAP core-shell NW corresponding to the coating cycles of 2, 7 and 20. As can be seen in these SEM images, the NW thickness gradually growth as the number of coatings increases. And, like anticipated, the

transparency of the electrode decreases through the Ppy coating as shown Figure 56 (d) and (e). Considering that the overall purpose of this study is to fabricate the transparent and stretchable supercapacitor, we would limit the coating process to 7cycle or less.

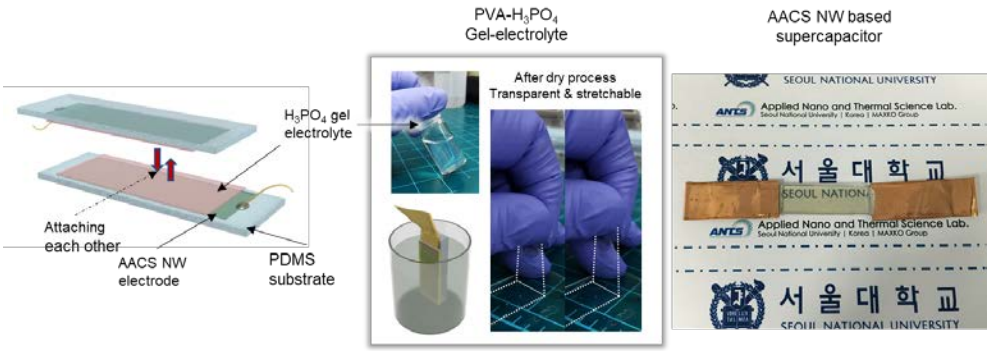

Figure 57. Fabrication of AAP NW based transparent and stretchable supercapacitor.

As shown in Figure 57, symmetric supercapacitors with two identical AAP core-shell NW electrodes are fabricated by attaching them with PVA-H_3PO_4 gel electrolyte. The supercapacitors fabricated with 3 coating cycle's AAP NW electrode show high transmittance as shown in Figure 57. This superior optical transmittance of the fabricated supercapacitor derives from the unique structure of the electrode which composed of NW network current collector and active layer directly and selectively deposited on the NW surface. Besides, it is anticipated that there is another benefit stem from the nanowire network structure, in terms of the energy storage ability of a supercapacitor. In the energy storage capacity or energy density of a supercapacitor, the specific surface area of the electrode is one of the most important factors. The surface area can vary greatly depending on the type of the material, even if the amount of the material is the same. Especially, when a material is present in the

form of a three-dimensional nanostructure, the surface area thereof increases severely and the AAP NW network is can be considered as such a three-dimensional nanostructure composed of two-dimensional NWs. To confirm this assumption, the same amount of PPy, which is controlled by monitoring the amount of consumed charge during the electro-polymerization, is electro-polymerized on the surface of AACS NW network electrode and sputter deposited Au film substrate. As shown in Figure 59 (a), although some hundreds nanometer sized sphere like aggregate are observed, the Ppy layer ultimately forms rough two-dimensional surface. On the contrary, the AACS NW network coated with the same amount of PPy shows three-dimensional NW network structure providing much larger surface area.

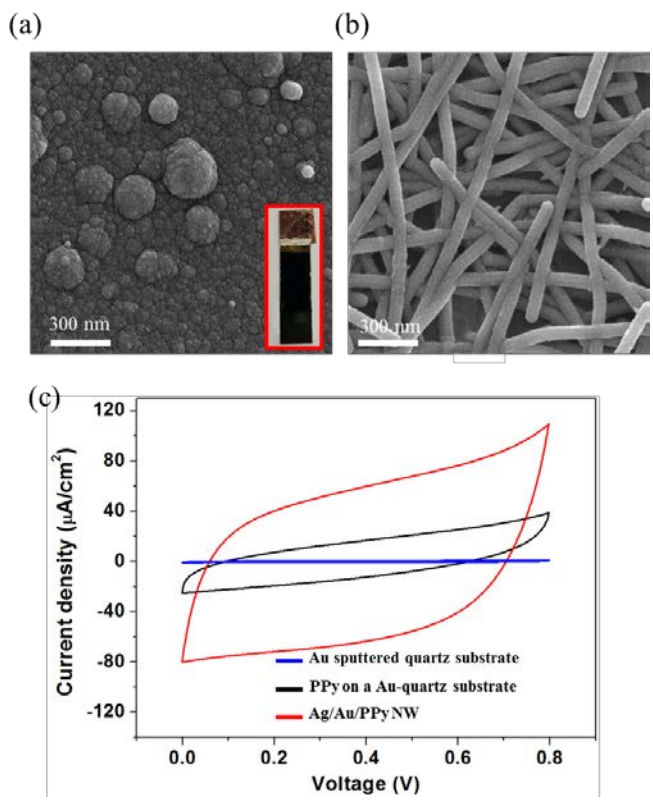

Figure 58. Comparison of the capacitance between thin film Ppy electrode and AAP NW network electrode.

Figure 58 (c) shows the CV curve of the supercapacitors that consists of bare flat Au-sputtered substrates, PPy-coated flat Au substrates and the AAP NW network electrode. Typically, a conducting polymer based supercapacitor stores the charges by incorporating anions into the polymer backbone, and here phosphate (PO_4^{3-}) ions are incorporated with positively charged PPy during the forward CV scan and they are detached from PPy during the discharging process. Due to this redox process, the electrodes coated with PPy exhibits larger current density than a pristine flat Au film (blue line). More importantly, the current density of the AAP NW supercapacitor is approximately three times larger than of the flat PPy film based supercapacitor, despite of the fixed amount of Ppy. It strongly supports the assumption that the nanowire network structure not only has the advantages of light transmittance but also can improve the energy storage density of supercapacitors by ensuring enlarged surface area.

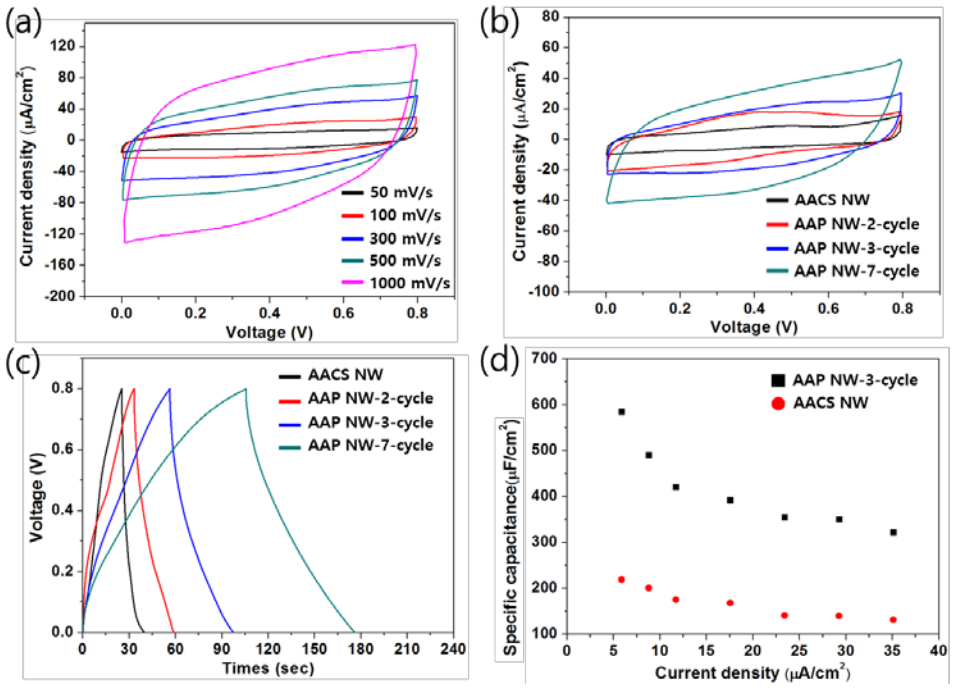

Figure 59. CV and Galvano-static measurement of AACS NW and AAP NW supercapacitor

Figure 59 (a) shows the CV curves for AAP-3-cycle NW supercapacitor at diverse voltage scan rates, from 50 mV/s to 1 V/s. The rectangular CV shape at 50 mV/s voltage scan rate maintains its shape until 1 V/s voltage scan rate. This rapid response characteristic seems to stem from fast electron transport through the AACS NW and tight coupling between the Au surfaces and PPy. Furthermore, the fast diffusion of electrolytes through the vacant area in the mesh structure enables a fully rectangular CV shape at a high scan rate. Figure 59 (b) showing CV curves of the AACS NW and AAP NW with different amounts of PPy exhibits that the capacitances of supercapacitor increase in proportion to the amount of PPy. In addition, the linear profile of the charge-discharge curves in Figure 59 (c) represent the ideal capacitive performance. Based on the charge-discharge graph and the

equation C = 2i/[A(⊿V/⊿t)], the areal capacitances are calculated where A is the geometric area of the electrode. These values increase by 75% and 270% as the number of PPy coating cycle increased to 2 and 3 cycles, respectively. This is a huge enhancement in terms of capacitance with minimal transmittance sacrifice of the supercapacitor considering the corresponding transmittance values are 81%, 77% and 65% respectively. Figure 59 (d) shows the areal capacitance at various current densities. The areal capacitance decreases from 580 μF/cm^2 to 320 μF/cm^2 as current density increases from 5.8 to 35 μA/cm^2. At such current densities, the AAP NW supercapacitor maintains 230% ~ 270% higher areal capacitance than the AACS NW supercapacitor. These values are comparable to the recently reported transparent[7] and high-performance[67] solid-state supercapacitors. Also, the specific capacitance of the supercapacitor considering only the PPy as the active material at the 5.8 μA/cm^2 current condition was 116.28 F/g. The obtained specific and areal capacitance values are similar or higher than those of many previously reported transparent and flexible supercapacitors using CNT, graphene and Au mesh with MnO_2. This is evidently due to the use of conducting polymer that uses the pseudo-capacitance mechanism and 3-dimensional structure of NW network mesh film with enhanced surface area.

After confirming the electrochemical properties of the AAP NW based supercapacitor, the reliability under mechanical stretching also investigated. CV measurement are conducted with AAP-3 cycle NW based supercapacitor against tensile strain up to 50%, as shown in insets of Figure 60. The CV curves are almost unchanged during the stretching test and this result demonstrates that the newly proposed AAP NW network structure can be used as a mechanically stable and stretchable energy storage device.

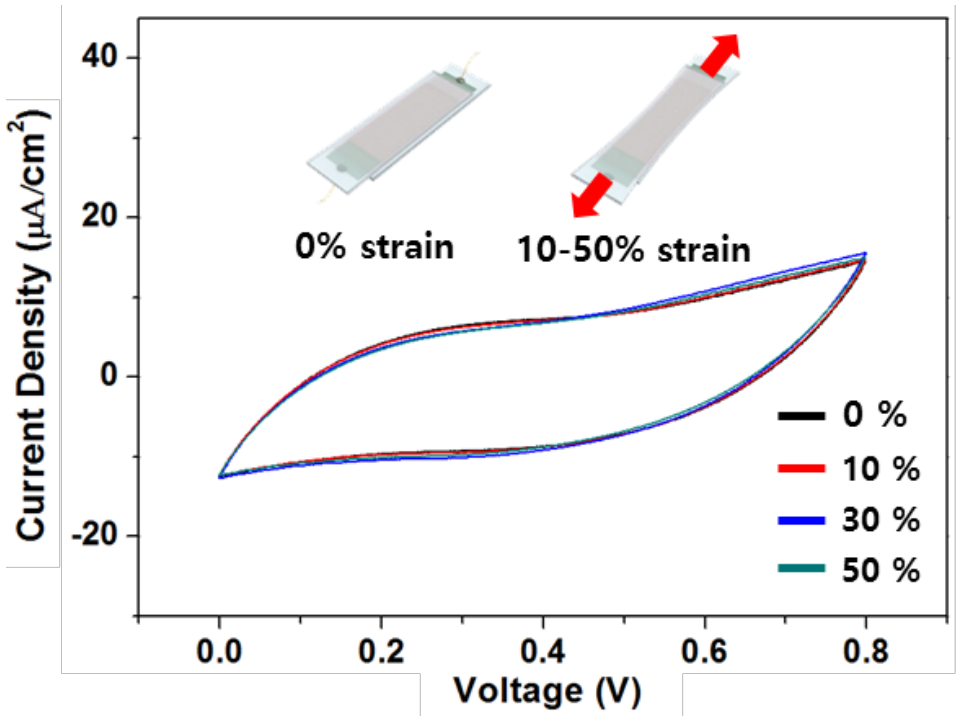

Figure 60. CV curves of AAP-3cycle NW supercapacitor at 50 mV/s voltage scan rate under various stretching condition.

Chapter 4. Summary and conclusion

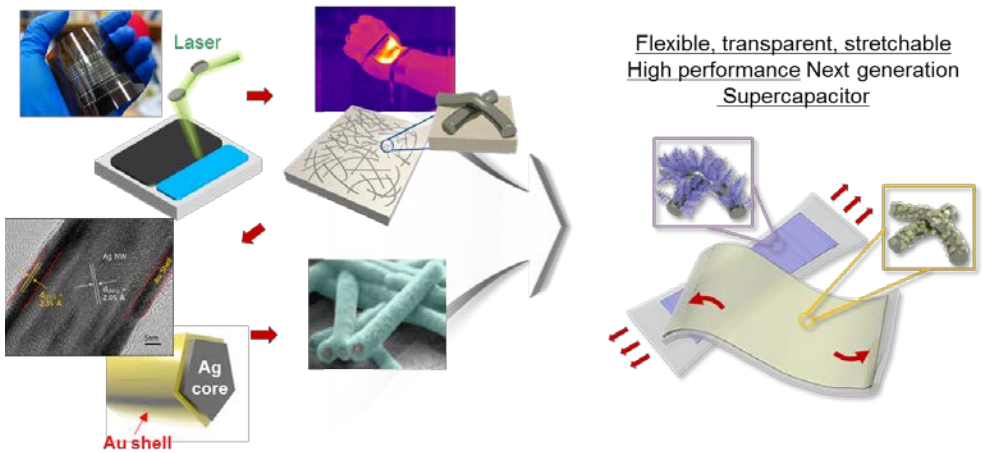

Figure 61. Schematic diagram of research flows of this work.

In this work, we have studied the fabrication of transparent, flexible and stretchable electrodes using metal nanoparticles and metal nanowires. We also tried to fabricate a next generation energy storage device based on the electrodes. First, in the case of metal nanoparticle-based electrodes, we have studied the fabrication of flexible electrodes without damaging the substrate at room temperature by combining the dramatic melting point reduction phenomena of metal nanoparticle at the nanoscale and the local heating characteristics of the laser. Furthermore, we have developed a transparent and stretchable electrode fabrication process using nanowire network structure and have developed the Ag-Au core shell nanowire (AACS NW) synthesis process that can greatly improve electrochemical stability, confirming the possibility of using nanowire network-based electrode as supercapacitor. Subsequently, Ppy layer is deposited on the surface of AACS NW to

form the Ag-Au-Ppy core shell NW (AAP NW). Finally, the AAP NW network / PDMS composite electrode is used for the higher performance transparent and stretchable supercapacitor. The resultant supercapacitor shows superior transmittance and stretchability comparing with the previous reported transparent and stretchable supercapacitors.

Material	Transparency (at 550nm)	Stretchability	Capacitance	Process
AACS NW	**73%**	**60%**	**210 μF/cm²**	**All solution process No pre-strain**
AAP NW	**66%**	**50%**	**680 μF/cm²**	**All solution process No pre-strain**
Graphene	60%	40%	7.6 mF/g, 5.8 μF/cm²	CVD / Winkled Cu foil Pre-strain
Graphene	46.5%	38%	1.55 mF/cm²	MPESCD, NaCl Free-standing
Graphene	No-transparent	50%	650 μF/cm²	Laser induced graphene
Au-MnO_2	36%	Flexible	795 μF/cm²	Evaporated Au coating with PS array Mask
CNT	75%	120%	17.5 F/g, 47.5 μF/cm²	Aerosol synthesis Pre-strain

Table 2. Comparison of this work with other previous researches about transparent, flexible and stretchable supercapacitor.

Bibliography

[1] S. Bai, C. Sun, P. Wan, C. Wang, R. Luo, Y. Li, *et al.*, "Transparent Conducting Films of Hierarchically Nanostructured Polyaniline Networks on Flexible Substrates for High-Performance Gas Sensors," *Small,* vol. 11, pp. 306-310, 2015.

[2] T. Q. Trung, S. Ramasundaram, B.-U. Hwang, and N.-E. Lee, "An All-Elastomeric Transparent and Stretchable Temperature Sensor for Body-Attachable Wearable Electronics," *Advanced Materials,* vol. 28, pp. 502-509, 2016.

[3] A. Zucca, C. Cipriani, Sudha, S. Tarantino, D. Ricci, V. Mattoli, *et al.*, "Conformable Electronics: Tattoo Conductive Polymer Nanosheets for Skin-Contact Applications (Adv. Healthcare Mater. 7/2015)," *Advanced Healthcare Materials,* vol. 4, pp. 941-941, 2015.

[4] J. Zhong, Y. Zhang, Q. Zhong, Q. Hu, B. Hu, Z. L. Wang, *et al.*, "Fiber-Based Generator for Wearable Electronics and Mobile Medication," *ACS Nano,* vol. 8, pp. 6273-6280, 2014/06/24 2014.

[5] S.-K. Kim, H. J. Kim, J.-C. Lee, P. V. Braun, and H. S. Park, "Extremely Durable, Flexible Supercapacitors with Greatly Improved Performance at High Temperatures," *ACS Nano,* vol. 9, pp. 8569-8577, 2015/08/25 2015.

[6] S. Dörfler, I. Felhösi, T. Marek, S. Thieme, H. Althues, L. Nyikos, *et al.*, "High power supercap electrodes based on vertical aligned carbon nanotubes on aluminum," *Journal of Power Sources,* vol. 227, pp. 218-228, 4/1/ 2013.

[7] J. Zhi, W. Zhao, X. Liu, A. Chen, Z. Liu, and F. Huang, "Highly conductive ordered mesoporous carbon based electrodes decorated by 3D graphene and 1D silver nanowire for flexible supercapacitor," *Advanced Functional Materials,* vol. 24, pp. 2013-2019, 2014.

[8] Y. Li, Z. Li, and P. K. Shen, "Simultaneous Formation of Ultrahigh Surface Area and Three-Dimensional Hierarchical Porous Graphene-Like Networks for Fast and Highly Stable Supercapacitors," *Advanced Materials,* vol. 25, pp. 2474-2480, 2013.

[9] J. Yeo, G. Kim, S. Hong, M. S. Kim, D. Kim, J. Lee, *et al.*, "Flexible supercapacitor fabrication by room temperature rapid laser processing of roll-to-roll printed metal nanoparticle ink for wearable electronics application," *Journal of Power Sources,* vol. 246, pp. 562-568, 2014.

[10] S. Pay and Y. Baghzouz, "Effectiveness of battery-supercapacitor combination in electric vehicles," in *Power Tech Conference Proceedings, 2003 IEEE Bologna*, 2003, p. 6 pp. Vol. 3.

[11] Q. Wang, Z. Wen, and J. Li, "A hybrid supercapacitor fabricated with a carbon nanotube cathode and a TiO2-B nanowire anode," *Advanced Functional Materials,* vol. 16, pp. 2141-2146, 2006.

[12] Y. Wang, Z. Shi, Y. Huang, Y. Ma, C. Wang, M. Chen, *et al.*, "Supercapacitor devices based on graphene materials," *The Journal of Physical Chemistry C,* vol. 113, pp. 13103-13107, 2009.

[13] A. Yu, V. Chabot, and J. Zhang, *Electrochemical Supercapacitors for Energy Storage and Delivery: Fundamentals and Applications*: CRC Press, 2013.

[14] H. Y. Jung, M. B. Karimi, M. G. Hahm, P. M. Ajayan, and Y. J. Jung, "Transparent, flexible supercapacitors from nano-engineered carbon films," *Scientific Reports,* vol. 2, p. 773, 10/26/online 2012.

[15] K. Jo, S. Lee, S.-M. Kim, J. B. In, S.-M. Lee, J.-H. Kim, *et al.*, "Stacked Bilayer Graphene and Redox-Active Interlayer for Transparent and Flexible High-Performance Supercapacitors," *Chemistry of Materials,* vol. 27, pp. 3621-3627, 2015/05/26 2015.

[16] Y. Z. Wang, Q. Wang, H. Y. Xie, L. P. Ho, D. M. F. Tan, Y. Y. Diao, *et al.*, "Fabrication of highly ordered P3HT:PCBM nanostructures and its application as a supercapacitive electrode," *Nanoscale,* vol. 4, pp. 3725-3728, 2012.

[17] L. Hu, M. Pasta, F. L. Mantia, L. Cui, S. Jeong, H. D. Deshazer, *et al.*, "Stretchable, porous, and conductive energy textiles," *Nano letters,* vol. 10, pp. 708-714, 2010.

[18] Y.-Y. Horng, Y.-C. Lu, Y.-K. Hsu, C.-C. Chen, L.-C. Chen, and K.-H. Chen, "Flexible supercapacitor based on polyaniline nanowires/carbon cloth with both high gravimetric and area-normalized capacitance," *Journal of Power Sources,* vol. 195,

pp. 4418-4422, 2010.
[19] Y.-H. Lee, Y. Kim, T.-I. Lee, I. Lee, J. Shin, H. S. Lee, *et al.*, "Anomalous Stretchable Conductivity Using an Engineered Tricot Weave," *ACS nano,* vol. 9, pp. 12214-12223, 2015.
[20] C. H. Lee, Y. Ma, K. I. Jang, A. Banks, T. Pan, X. Feng, *et al.*, "Soft Core/Shell Packages for Stretchable Electronics," *Advanced Functional Materials,* vol. 25, 2015.
[21] S. Lim, D. Son, J. Kim, Y. B. Lee, J. K. Song, S. Choi, *et al.*, "Transparent and Stretchable Interactive Human Machine Interface Based on Patterned Graphene Heterostructures," *Advanced Functional Materials,* vol. 25, pp. 375-383, 2015.
[22] G. Gruner, "Carbon nanotube films for transparent and plastic electronics," *J. Mater. Chem.,* vol. 16, pp. 3533-3539, 2006.
[23] K. S. Kim, Y. Zhao, H. Jang, S. Y. Lee, J. M. Kim, K. S. Kim, *et al.*, "Large-scale pattern growth of graphene films for stretchable transparent electrodes," *Nature,* vol. 457, pp. 706-710, 2009.
[24] T.-M. Lee, S.-H. Lee, J.-H. Noh, D.-S. Kim, and S. Chun, "The effect of shear force on ink transfer in gravure offset printing," *Journal of Micromechanics and Microengineering,* vol. 20, p. 125026, 2010.
[25] M. Kaempgen, C. K. Chan, J. Ma, Y. Cui, and G. Gruner, "Printable thin film supercapacitors using single-walled carbon nanotubes," *Nano letters,* vol. 9, pp. 1872-1876, 2009.
[26] Z.-S. Wu, W. Ren, D.-W. Wang, F. Li, B. Liu, and H.-M. Cheng, "High-energy MnO2 nanowire/graphene and graphene asymmetric electrochemical capacitors," *ACS nano,* vol. 4, pp. 5835-5842, 2010.
[27] C. Zhou and J. Liu, "Carbon nanotube network film directly grown on carbon cloth for high-performance solid-state flexible supercapacitors," *Nanotechnology,* vol. 25, p. 035402, 2014.
[28] F. Meng and Y. Ding, "Sub-Micrometer-Thick All-Solid-State Supercapacitors with High Power and Energy Densities," *Advanced Materials,* vol. 23, pp. 4098-4102, 2011.
[29] C. Meng, C. Liu, L. Chen, C. Hu, and S. Fan, "Highly flexible and all-solid-state paperlike polymer supercapacitors," *Nano letters,* vol. 10, pp. 4025-4031, 2010.
[30] J. Yeo, S. Hong, M. Wanit, H. W. Kang, D. Lee, C. P. Grigoropoulos, *et al.*, "Rapid, one-step, digital selective growth of ZnO nanowires on 3D structures using laser induced hydrothermal growth," *Advanced Functional Materials,* vol. 23, pp. 3316-3323, 2013.
[31] S. Hong, J. Yeo, W. Manorotkul, G. Kim, J. Kwon, K. An, *et al.*, "Low-temperature rapid fabrication of ZnO nanowire UV sensor array by laser-induced local hydrothermal growth," *Journal of Nanomaterials,* vol. 2013, p. 2, 2013.
[32] J. Kwon, S. Hong, H. Lee, J. Yeo, S. S. Lee, and S. H. Ko, "Direct selective growth of ZnO nanowire arrays from inkjet-printed zinc acetate precursor on a heated substrate," *Nanoscale research letters,* vol. 8, pp. 1-6, 2013.
[33] J. Yeo, S. Hong, D. Lee, N. Hotz, M.-T. Lee, C. P. Grigoropoulos, *et al.*, "Next generation non-vacuum, maskless, low temperature nanoparticle ink laser digital direct metal patterning for a large area flexible electronics," *PloS one,* vol. 7, p. e42315, 2012.
[34] D. R. Cairns, R. P. Witte Ii, D. K. Sparacin, S. M. Sachsman, D. C. Paine, G. P. Crawford, *et al.*, "Strain-dependent electrical resistance of tin-doped indium oxide on polymer substrates," *Applied Physics Letters,* vol. 76, pp. 1425-1427, 2000.
[35] J. Liu, D. Wu, and S. Zeng, "Influence of temperature and layers on the characterization of ITO films," *Journal of Materials Processing Technology,* vol. 209, pp. 3943-3948, 2009.
[36] K. K. Kim, S. Hong, H. M. Cho, J. Lee, Y. D. Suh, J. Ham, *et al.*, "Highly Sensitive and Stretchable Multidimensional Strain Sensor with Prestrained Anisotropic Metal Nanowire Percolation Networks," *Nano Letters,* vol. 15, pp. 5240-5247, 2015/08/12 2015.
[37] J. Lee, P. Lee, H. B. Lee, S. Hong, I. Lee, J. Yeo, *et al.*, "Room-Temperature Nanosoldering of a Very Long Metal Nanowire Network by Conducting-Polymer-Assisted Joining for a Flexible Touch-Panel Application," *Advanced Functional Materials,* vol. 23, pp. 4171-4176, 2013.
[38] J. Jiu, T. Araki, J. Wang, M. Nogi, T. Sugahara, S. Nagao, *et al.*, "Facile synthesis of

very-long silver nanowires for transparent electrodes," *Journal of Materials Chemistry A,* vol. 2, pp. 6326-6330, 2014.
[39] S. S. Velankar, V. Lai, and R. A. Vaia, "Swelling-Induced Delamination Causes Folding of Surface-Tethered Polymer Gels," *ACS Applied Materials & Interfaces,* vol. 4, pp. 24-29, 2012/01/25 2011.
[40] M. J. Neeson, R. R. Dagastine, D. Y. C. Chan, and R. F. Tabor, "Evaporation of a capillary bridge between a particle and a surface," *Soft Matter,* vol. 10, pp. 8489-8499, 2014.
[41] E. C. Garnett, W. Cai, J. J. Cha, F. Mahmood, S. T. Connor, M. Greyson Christoforo, *et al.*, "Self-limited plasmonic welding of silver nanowire junctions," *Nat Mater,* vol. 11, pp. 241-249, 2012.
[42] S. Han, S. Hong, J. Ham, J. Yeo, J. Lee, B. Kang, *et al.*, "Fast Plasmonic Laser Nanowelding for a Cu-Nanowire Percolation Network for Flexible Transparent Conductors and Stretchable Electronics," *Advanced Materials,* vol. 26, pp. 5808-5814, 2014.
[43] J. C. McDonald and G. M. Whitesides, "Poly(dimethylsiloxane) as a Material for Fabricating Microfluidic Devices," *Accounts of Chemical Research,* vol. 35, pp. 491-499, 2002/07/01 2002.
[44] S. Hong, J. Yeo, J. Lee, H. Lee, P. Lee, S. S. Lee, *et al.*, "Selective Laser Direct Patterning of Silver Nanowire Percolation Network Transparent Conductor for Capacitive Touch Panel," *Journal of Nanoscience and Nanotechnology,* vol. 15, pp. 2317-2323, 2015.
[45] S.-K. Kim, H. J. Kim, J.-C. Lee, P. V. Braun, and H. S. Park, "Extremely Durable, Flexible Supercapacitors with Greatly Improved Performance at High Temperatures," *ACS nano,* 2015.
[46] M.-S. Lee, K. Lee, S.-Y. Kim, H. Lee, J. Park, K.-H. Choi, *et al.*, "High-performance, transparent, and stretchable electrodes using graphene-metal nanowire hybrid structures," *Nano letters,* vol. 13, pp. 2814-2821, 2013.
[47] U. Kim, J. Kang, C. Lee, H. Y. Kwon, S. Hwang, H. Moon, *et al.*, "A transparent and stretchable graphene-based actuator for tactile display," *Nanotechnology,* vol. 24, p. 145501, 2013.
[48] Y. Yang, S. Jeong, L. Hu, H. Wu, S. W. Lee, and Y. Cui, "Transparent lithium-ion batteries," *Proceedings of the National Academy of Sciences,* vol. 108, pp. 13013-13018, 2011.
[49] J. Yu, W. Lu, S. Pei, K. Gong, L. Wang, L. Meng, *et al.*, "Omnidirectionally Stretchable High Performance Supercapacitor Based on Isotropic Buckled Carbon Nanotube Films," *ACS nano,* 2016.
[50] A. Lamberti, F. Clerici, M. Fontana, and L. Scaltrito, "A Highly Stretchable Supercapacitor Using Laser-Induced Graphene Electrodes onto Elastomeric Substrate," *Advanced Energy Materials,* 2016.
[51] K. Zhang, L. L. Zhang, X. Zhao, and J. Wu, "Graphene/polyaniline nanofiber composites as supercapacitor electrodes," *Chemistry of Materials,* vol. 22, pp. 1392-1401, 2010.
[52] C.-H. Liu and X. Yu, "Silver nanowire-based transparent, flexible, and conductive thin film," *Nanoscale Res. Lett,* vol. 6, p. 75, 2011.
[53] J. Lee, P. Lee, H. Lee, D. Lee, S. S. Lee, and S. H. Ko, "Very long Ag nanowire synthesis and its application in a highly transparent, conductive and flexible metal electrode touch panel," *Nanoscale,* vol. 4, pp. 6408-6414, 2012.
[54] T. Akter and W. S. Kim, "Reversibly stretchable transparent conductive coatings of spray-deposited silver nanowires," *ACS applied materials & interfaces,* vol. 4, pp. 1855-1859, 2012.
[55] M. Giovanni and M. Pumera, "Size Dependant Electrochemical Behavior of Silver Nanoparticles with Sizes of 10, 20, 40, 80 and 107 nm," *Electroanalysis,* vol. 24, pp. 615-617, 2012.
[56] N. Murshid, I. Gourevich, N. Coombs, and V. Kitaev, "Gold plating of silver nanoparticles for superior stability and preserved plasmonic and sensing properties," *Chemical Communications,* vol. 49, pp. 11355-11357, 2013.
[57] H. Lee, S. Hong, J. Kwon, Y. D. Suh, J. Lee, H. Moon, *et al.*, "All-solid-state flexible supercapacitors by fast laser annealing of printed metal nanoparticle layers," *Journal of Materials Chemistry A,* vol. 3, pp. 8339-8345, 2015.

[58] S. Li, Y. Shen, A. Xie, X. Yu, L. Qiu, L. Zhang, *et al.*, "Green synthesis of silver nanoparticles using Capsicum annuum L. extract," *Green Chem.,* vol. 9, pp. 852-858, 2007.
[59] Y. Jin, C. Jia, S.-W. Huang, M. O'Donnell, and X. Gao, "Multifunctional nanoparticles as coupled contrast agents," *Nature communications,* vol. 1, p. 41, 2010.
[60] T. Chen, H. Peng, M. Durstock, and L. Dai, "High-performance transparent and stretchable all-solid supercapacitors based on highly aligned carbon nanotube sheets," *Scientific reports,* vol. 4, 2014.
[61] F. Mohammad, P. D. Calvert, and N. C. Billingham, "Thermal stability of electrochemically prepared polythiophene and polypyrrole," *Bulletin of Materials Science,* vol. 18, pp. 255-261, 1995.
[62] V.-T. Truong, B. C. Ennis, T. G. Turner, and C. M. Jenden, "Thermal stability of polypyrroles," *Polymer International,* vol. 27, pp. 187-195, 1992.
[63] H. Wei, C. He, J. Liu, H. Gu, Y. Wang, X. Yan, *et al.*, "Electropolymerized polypyrrole nanocomposites with cobalt oxide coated on carbon paper for electrochemical energy storage," *Polymer,* vol. 67, pp. 192-199, 6/12/ 2015.
[64] H. Tang, J. Wang, H. Yin, H. Zhao, D. Wang, and Z. Tang, "Growth of Polypyrrole Ultrathin Films on MoS2 Monolayers as High-Performance Supercapacitor Electrodes," *Advanced Materials,* vol. 27, pp. 1117-1123, 2015.
[65] L. Yuan, B. Yao, B. Hu, K. Huo, W. Chen, and J. Zhou, "Polypyrrole-coated paper for flexible solid-state energy storage," *Energy & Environmental Science,* vol. 6, pp. 470-476, 2013.
[66] H. R. Kricheldorf, *Handbook of polymer synthesis* vol. 24: CRC Press, 1991.
[67] M. Huang, Y. Zhang, F. Li, Z. Wang, N. Hu, Z. Wen, *et al.*, "Merging of Kirkendall growth and Ostwald ripening: CuO@ MnO2 core-shell architectures for asymmetric supercapacitors," *Scientific reports,* vol. 4, 2014.

Abstract

금속 나노와이어 그물망 전극 기반의 고신축성 투명 슈퍼캐패시터 제작

이하범 (李 昰 範, Lee, Habeom)
기계항공공학부 기계공학전공
서울대학교

휴대용 전자 기기에 대한 소비자의 요구가 다양해짐에 따라, 투명하고 유연하며 심지어 신축성을 갖는 전자 기기에 대한 수요가 날로 증가하고 있다. 모든 전자 기기에 있어 에너지 저장 및 공급 장치는 필수 요소이며 고려될 수 있는 다양한 에너지 장치들 중, 슈퍼캐패시터는 큰 에너지 밀도, 빠른 충방전 속도, 뛰어난 안전성, 우수한 휴대성 등과 같은 다양한 장점들을 갖는다.

본 연구는, 기존의 단단하고 고정된 형태의 슈퍼캐패시터에서 벗어나, 투명하면서도 굽힘, 뒤틀림, 늘림과 같은 물리적 변형 조건 하에서도 본래의 성능을 유지할 수 있는 차세대 슈퍼캐패시터 제작을 목표로 하였다. 가장 먼저, 유연 기판 상에 도포된 은 나노 입자의 레이저 소결 공정을 통해 유연 기판에 열 손상을 주지 않는 저온 조건에서 유연 전극을 제작할 수 있는 기술을 개발하였으며, 해당 기술을 롤투롤 인쇄 공정의 후처리 공정으로 활용하여 유연전극의 생산성을 향상시킬 수 있음을 보였다.

나아가, 광 투과성을 갖는 신축성 기판 상에 은 나노 와이어 그물망 구조를 간단하게 형성할 수 있는 공정을 확립하고 그 원리를 설명함으로써, 신축성 투명 전극 제작 공정을 확립하였다. 해당 전극을 활용하여 투명하면서도 신축성을 갖는 신개념 히터를 제작하여 은 나노와이어 그물망 전극의 웨어러블 전자 기기로의 활용 가능성을

입증하였으며 은 나노 와이어 표면에 금 박막을 코팅할 수 있는 용액 공정을 개발하여 은 나노 와이어 그물망 전극의 화학적, 전기 화학적 안정성을 향상시킴으로써 60% 의 인장 조건 하에서도 성능을 유지할 수 있는 신축성, 투명 슈퍼캐패시터 제작에 성공하였다. 또한 전도성 폴리머를 금속 나노와이어 표면에 선택적으로 코팅하여 해당 슈퍼캐패시터의 성능을 더욱 향상시킬 수 있음을 보였다.

이상의 과정을 통해 은 나노입자 및 은 나노와이어를 활용한 유연, 투명, 신축성 전극 제작 공정을 확립하고 해당 전극을 활용하여 신축성 투명 히터, 나아가 신축성 투명 슈퍼캐패시터를 제작함으로써, 금속 나노물질을 활용한 차세대 웨어러블 전자기기 제조 기술 개발에 기여하였다.

주요어 : 은 나노입자, 레이저 소결 공정, 은 나노와이어, 금-은 코어쉘 나노와이어, 신축성 투명 전극, 신축성 투명 슈퍼캐패시터
학 번 : 2014-30337